PB97-129555

COMPARISON OF FIRE MODEL PREDICTIONS WITH EXPERIMENTS CONDUCTED IN A HANGAR WITH A 15 METER CEILING

(U.S.) NATIONAL INST. OF STANDARDS AND TECHNOLOGY (BFRL)
GAITHERSBURG, MD

DEC 96

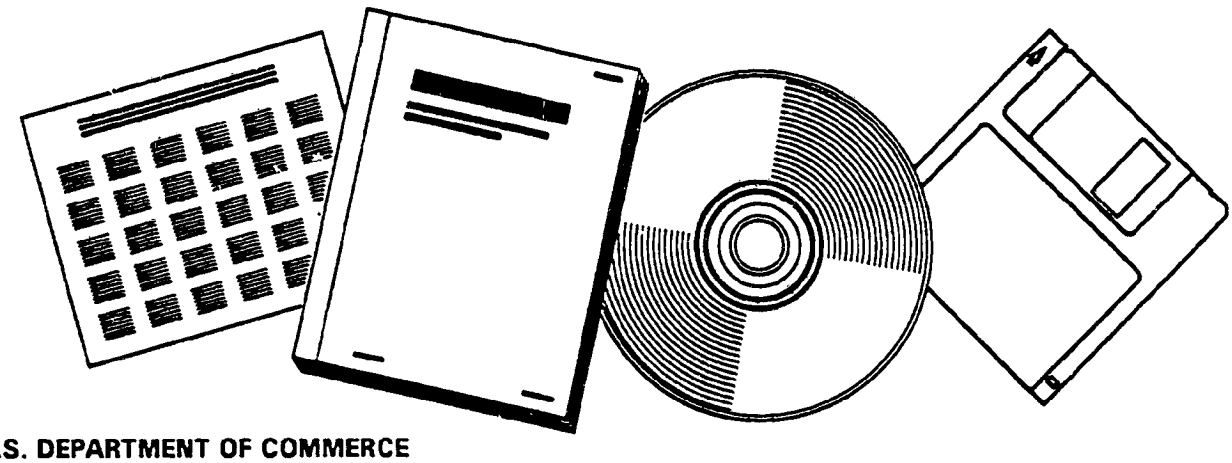

U.S. DEPARTMENT OF COMMERCE
National Technical Information Service

NISTIR 5927

COMPARISON OF FIRE MODEL PREDICTIONS WITH EXPERIMENTS CONDUCTED IN A HANGAR WITH A 15 METER CEILING

William D. Davis, Kathy A. Notarianni and K. B. McGrattan

United States Department of Commerce
Technology Administration
National Institute of Standards and Technology

NISTIR 5927

COMPARISON OF FIRE MODEL PREDICTIONS WITH EXPERIMENTS CONDUCTED IN A HANGAR WITH A 15 METER CEILING

William D. Davis, Kathy A. Notarianni, and K. B. McGrattan
Building and Fire Research Laboratory
National Institute of Standards and Technology
Gaithersburg, MD 20899

December 1996

U.S. Department of Commerce
Michael Kantor, *Secretary*
Technology Administration
Mary L. Good, *Under Secretary for Technology*
National Institute of Standards and Technology
Arati Prabhakar, *Director*

Prepared for:
National Aeronautics and Space Administration
NASA Headquarters
Office of Safety and
Mission Assurance

COMPARISON OF FIRE MODEL PREDICTIONS WITH EXPERIMENTS CONDUCTED IN A HANGAR WITH A 15 m CEILING

W. D. Davis, K. A. Notarianni, and K. B. McGrattan

1.0 INTRODUCTION

Spaces with high ceilings, such as warehouses, atriums, clean rooms, and aircraft hangars, represent some of the most difficult fire protection challenges since they can contain large quantities of fuel, house valuable equipment or airplanes, have unique geometries, and present special life safety problems. The fire protection problem at heights in excess of 10 m is made more difficult by the lack of verification studies for computer fire models. Computer fire models could be used by fire protection engineers to aid in the fire detection design of the facility. Without appropriate verification studies, the accuracy of computer model predictions is uncertain and the application of these models to fire problems becomes questionable.

The purpose of this study is to examine the predictive capabilities of fire models using the results of a series of fire experiments conducted in an aircraft hangar with a ceiling height of about 15 m. The National Aeronautics and Space Administration (NASA), which funded this study, was interested in computer fire model verification at heights above 10 m such that computer models could be used to analyze fire protection strategies in their high ceiling spaces. The fire experiments were conducted at Barbers Point, Hawaii by NIST in conjunction with the Naval Facilities Engineering Command (NAVFAC) [1].

This study is designed to investigate model applicability at a ceiling height where only a limited amount of experimental data is available. Some earlier efforts to compare computer models with experimental data at heights above 14 m include those of Walton [2], Duong [3] and Notarianni and Davis [4]. This analysis deals primarily with temperature comparisons as a function of distance from the fire center and depth beneath the ceiling. Only limited velocity measurements in the ceiling jet were available but these are also compared with those models with a velocity predictive capability. The fire models included in the study are the plume correlations of Heskestad [5] and McCaffrey [6], the ceiling jet correlation of Alpert [7], the zone models CFAST [8], FPEtool [9], and LAVENT [10], and the CFD models CFX [11] and NIST-LES [12].

2.0 Barbers Point Experiments

Fire experiments were conducted in a Navy hangar at Barbers Point, Hawaii in order to test a number of fire detection devices which could be used to detect fires in large spaces. The hangar had a maximum ceiling height of 15.1 m (50 ft) with floor dimensions of 97.8 m by 73.8 m.

Figure 1 shows a plan view of the hangar with test east shown on the figure. All directions given in the paper are referenced to test east.

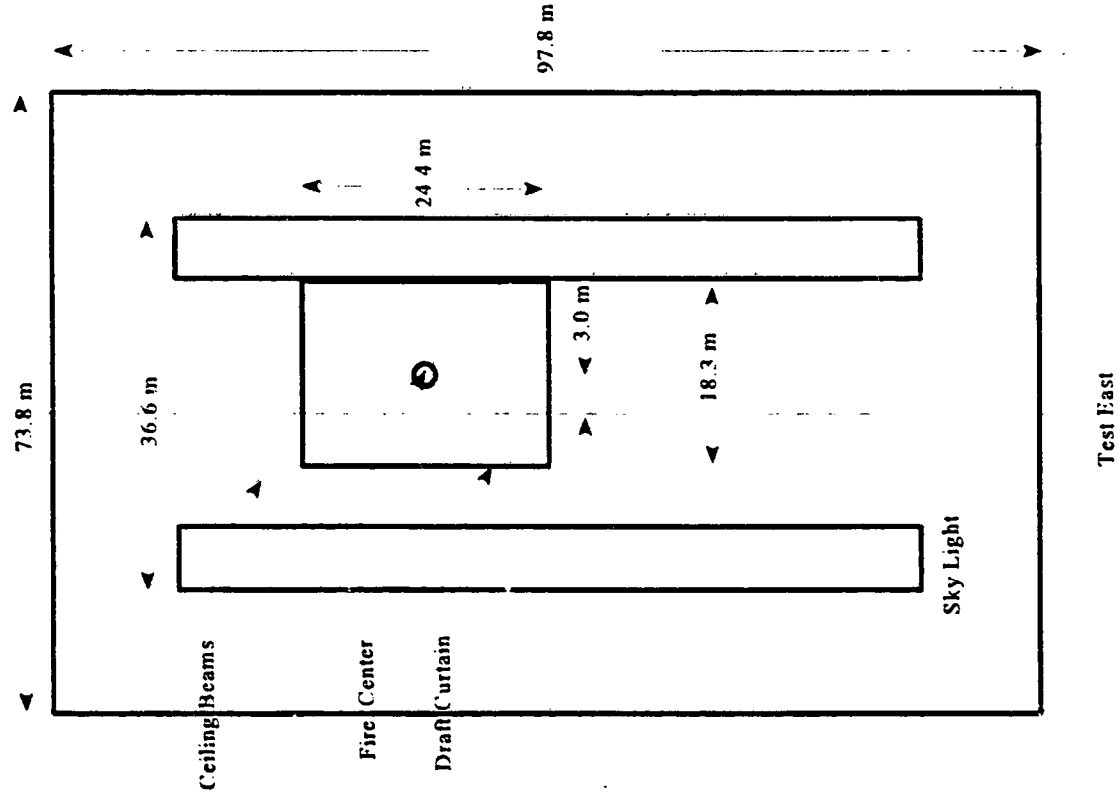

Figure 1 Plan View of Hangar

The experimental fires were located at the floor of the hangar and were positioned 12.2 m from the center of the hangar in the west direction. The height of the roof at this point is 14.9 m. The roof exhibits a 3 degree slope up toward the east direction. The roof consists of built-up tar and gravel over a corrugated metal deck. The metal deck is directly supported by 0.25 m high I-beams which run the width of the hangar in the north-south direction and are spaced 4.1 m on center. The I-beams are supported by open steel trusses which run perpendicular to the beams and are spaced 6.1 m on center. These trusses span the full length of the hangar.

There are no permanent draft curtains in the hangar. A temporary draft curtain made of fire retardant canvas was constructed for the fire experiments modeled here. The space between the

top edge of the draft curtain and the metal deck was sealed with glass fiber insulation to prevent smoke leakage beyond the top of the curtain The draft curtain area measured 24.4 m in length, 18.3 m in width, and 3.7 m in depth. The test fires were centered within the draft curtained area.

The ceiling height at the west edge of the draft curtain was 14.2 m.
The hangar has no existing heating or air conditioning system. During the tests studied here, the hangar doors at the east and west ends of the hangar were closed as were the louvered glass openings in the two skylights.

Sixty four thermocouples were installed in the hangar in order to measure gas and fuel temperatures. The position of the plume was defined using an array of five thermocouples which were placed 0.31 m below the ceiling with one on the center line and the other four installed 1.5 m from the center in the experimental north, south, east and west directions. In addition, nine thermocouples were installed 3.0 m below the ceiling in a cross pattern, one along the centerline and two radially out from the center in each of the four directions at 0.91 m and 2.1 m. Two additional thermocouples were installed 1.5 m and 6.1 m below the ceiling along the centerline.

Additional thermocouples used to define the radial temperature variation of the ceiling jet were located 0.31 m below the ceiling 1.5 m, 3.0 m, 6.1 m, 9.1 m and 11.6 m radially out from the center to the east and west and 1.5 m, 3.0 m, 6.1 m, and 8.5 m radially out from the center in the north and south directions. Thermocouples located radially 6.1 m in all four directions and 9.1 m in the east at 0.15 m, 0.30 m 0.46 m, 0.61 m, and 0.76 m were used to define the vertical temperature distribution of the ceiling jet. Additional thermocouples were located 3.0 m beneath the ceiling 8.5 m north and 9.1 m east of center to measure the filling time for the draft curtain.

Hot gas flow into areas adjacent to the draft curtain was monitored using thermocouples located 11.6 m to the north, 11.6 m and 14.6 m to the south, and 14.6 m and 17.7 m to the east and west. Each of these thermocouples was located at a distance of 0.31 m beneath the ceiling. The north thermocouple at 11.6 m was located inside one of the skylights.

Ceiling jet velocity was measured using two Sierra Steel-Trak industrial insertion mass flow meters (series 640). These were located 6.1 m radially to the north and east and were positioned 0.3 m beneath the ceiling. Additional details of the instrumentation may be found in reference 1.

Eleven JP-5 pan fire tests were conducted at this facility. Of the eleven tests, test 2 and test 4 were chosen to model since reliable heat release rate information was available and the fire plume in each of these tests was well behaved and exhibited a minimum of lean. Test 2 used a 0.6 m square pan which generated a maximum heat release rate of 500 kW. Test 4 involved a round pan with a diameter of 1.5 m, which yielded a maximum heat release rate of 2.7 MW. Both tests were conducted with the draft curtain in place. These fires will be referred to as the 500 kW and 2.7 MW fires for the duration of the paper.

3.0 Fire Models

The ability to predict temperature, smoke depth and density, gas flow and a variety of other fire related phenomena has improved dramatically over the last decade. Typical predictive models range from simple correlations of experimental data to sophisticated computer models which solve the conservation equations for mass, momentum, and energy over a fine grid. The deterministic computer models are divided into two general classifications: zone models and field models; the latter are also referred to as computational fluid dynamics (CFD) models.

The zone models generally divide the fire compartment into two zones, or control volumes, usually designated as an upper and lower layer. The gas temperature and density are assumed to be constant in each zone. The conservation laws for mass and energy are solved in time with the fire modeled as a release of energy and mass in one of the layers. Mass and energy transfer between layers is accomplished using plume models which are typically correlations derived from experimental data. Energy and mass flow into adjacent compartments is done using hydrostatic pressure differences between the compartments as a function of height. Additional information regarding the theoretical approximations used in zone models may be obtained from reference [13].

The CFD models solve the conservation equations for mass, momentum and energy in differential form by dividing the fire compartment into many control volumes and solving the resulting algebraic equations in time. The fire may be introduced either as a heat source into one or more control volumes or as Lagrangian particles representing burning fuel, with the resulting gas flow determined locally throughout the computational domain. A major difference among CFD models is how each calculates the viscosity used in the momentum equation. Fire driven flows are typically turbulent in nature. The turbulence affects both the gas viscosity and the heat transfer in the gas. Two computer models that utilize different methods to model the turbulent effects are investigated. The first model [11] uses the standard k-ϵ method [14] to approximate the turbulent energy and dissipation produced by the fire. The use of this model eliminates the need for large numbers of control volumes which would be necessary to model the small scale turbulence. The second model [12] uses many control volumes in order to follow the turbulence down to a certain scale size which is determined by the size of the control volumes. Additional details of these models will be given in sections 3.3.1 and 3.3.2.

3.1 Correlations

3.1.1 Plume Models

Temperatures and velocities along the centerline of the fire plumes can be calculated from a number of different experimentally based correlations. Two correlations are tested here. The first is due to Heskestad [5]. This correlation predicts that the centerline temperature, T, and velocity u, are given as a function of height, z, by

$$T = T_\infty + 9.1[T_\infty/(gc_p^2\rho_\infty^2)]^{1/3}\dot{Q}_c^{2/3}(z-z_o)^{-5/3} \quad (1)$$

and

$$u = 3.4[g/(c_p\rho_\infty T_\infty)]^{1/3}Q_c^{1/3}(z-z_o)^{-1/3} \quad (2)$$

where T_∞ is the environmental temperature, g is the acceleration due to gravity, c_p and ρ_∞ are the specific heat and density of the surrounding air. $\dot{Q}_c$ is the convective heat release rate, and z_o is the virtual origin.

The elevation of the virtual origin below the fire source is given by

$$z_c = -1.02D + 0.083Q^{2/5} \quad (3)$$

where D is the diameter of the pool.

The second correlation is due to McCaffrey [6]. For the plume region where the temperature excess is 320 °C or less, the centerline temperature and velocity are given by

$$T = T_\infty + 0.75\frac{T_\infty}{g}\left(\frac{z}{\dot{Q}^{2/5}}\right)^{-5/3} \quad (4)$$

and

$$u = 1.1\left(\frac{\dot{Q}}{z}\right)^{1/3} \quad (5)$$

where $\dot{Q}$ is the total heat release rate.

3.1.2 Ceiling Jet Correlation

The ceiling jet correlation that is investigated is due to Alpert [7] and provides the following relations for maximum ceiling jet temperature and maximum ceiling jet velocity, U, as a function of radial distance, r, from the plume centerline:

$$T_{max} = T_\infty + 16.9\frac{\dot{Q}^{2/3}}{H^{5/3}};\ r/H \le 0.18 \quad (6)$$

$$T_{max} = T_\infty + 5.38\frac{(\dot{Q}/r)^{2/3}}{H};\ r/H > 0.18 \quad (7)$$

H is the ceiling height.

$$u = 0.195\frac{\dot{Q}^{1/3}H^{1/2}}{r^{5/6}};\ r/H > 0.15 \quad (8)$$

This correlation is used in computer programs DETACT-QS [15] and in FPEtool [9].

3.2 Zone Models

3.2.1 CFAST

CFAST [8] is a multi room zone fire model in which each room is divided into two control volumes, the upper and lower layers. The correlation used to model the transport of mass to the upper layer from the lower layer is the McCaffrey plume [16]. For plumes where the height to the upper layer is large and the fire size is small, the amount of mass entrained into the plume, m_e, is limited by the relation [8]

$$\dot{m}_e < \frac{\dot{Q}}{c_p(T_u - T_l)} \quad (9)$$

The ceiling jet model used in CFAST was developed by Cooper [17] and is similar to the model used in the zone model LAVENT. The major difference in the application of this algorithm in the two zone models is that LAVENT uses a different plume model and a different method of calculating heat transfer to the ceiling compared with CFAST. The ceiling jet model takes into account the impact of the upper layer on the plume and allows the temperature and velocity of the ceiling jet to vary with distance beneath the ceiling.

The most recent release of this model is called FASTLite [18] which provides the user with the same predictive physical models as are found in CFAST. The version of CFAST used in this study contains additional output features which enable the user to study the ceiling jet. Early comparisons of the predictions of CFAST to the experiments indicated that CFAST was predicting temperatures which were significantly higher than the measurements. It was discovered that the plume algorithm was using the total heat release rate rather than the convective heat release rate [19]. For the model comparisons used in this paper, the convective heat release rate is correctly used in the plume algorithm.

3.2.2 FPEtool

FPEtool [9] is made up of a number of modules which allow the user to access different correlations or use Fire Simulator, which is based on a simple two volume zone model, ASETBX. Fire Simulator can be used to estimate smoke and heat detector activations and has the capability to approximate the impact of a growing layer on detector activation.

Two ceiling jet temperature and velocity correlations are used in FPEtool. The first correlation is designed to estimate conservatively the damage caused by the hot plume gases The ceiling plume temperature calculated in this model is found from a correlation developed by Alpert and Ward [21]. The temperature as a function of radius from the assumed axisymmetric plume is given by

$$T = T_\infty + 22.2\dot{Q}^{2/3}/z^{5/3}; \; for \; \frac{r}{z} \le 0.2 \qquad \textbf{(10)}$$

The heat release rate is assumed constant and a hot layer of gas has been assumed to be not developed at the ceiling. This correlation normally leads to over prediction of the temperature at the ceiling.

The ceiling jet temperature as a function of radius is given by

$$T = T_\infty + 6.81\frac{(\frac{\dot{Q}}{r})^{2/3}}{z}; \; for \; \frac{r}{z} > 0.2 \qquad (11)$$

The second correlation available in FPEtool is designed to calculate the thermal response of a detector or sprinkler located near the ceiling in an area where a smoke layer does not develop. This correlation is the same correlation [7] that is used in DETACT-QS. FPEtool also accounts for the development of a layer using this algorithm by replacing the heat release rate and ceiling height of the original algorithm by a pseudo-fire positioned near the layer interface. Details of this algorithm may be found in reference 11.

An atrium smoke temperature correlation is also available in FPEtool which is based on the ASETBX plume equation [21]. The temperature rise in the atrium hot gas layer is given by

$$T_{atria} = \frac{220}{1+39.8(\frac{z^{5/3}}{\dot{Q}^{2/3}})} \qquad (12)$$

3.2.3 LAVENT

LAVENT is a single room zone fire model where the room is divided into two control volumes or layers. The model is designed to be used in situations where draft curtains at the ceiling contain the smoke flow and ceiling venting is available to control the smoke. The plume model used to calculate the mass entrainment in the lower layer is due to Heskestad [5] and the impact on the energy flow and entrainment in the upper layer is also included [22]. The temperature and velocity of the ceiling jet depend on the location beneath the ceiling as well as the radial location from fire center.

3.3 CFD Models

The numerical modeling of turbulent flows can be accomplished by either solving the time averaged Navier Stokes equations with a turbulence model or by solving the Navier Stokes equations using a grid resolution sufficient to simulate most or all of the important turbulent scales. When only large scale turbulence is simulated, the model is called a large eddy simulation and a turbulence model may be used to simulate the effects of turbulence on scales smaller than the grid resolution. Two CFD models are compared in this paper. The model CFX [11] uses the first approach to simulate turbulent flow, while the model NIST-LES uses the second approach.

3.3.1 CFX

The CFD model CFX (formerly designated HARWELL FLOW3D) solves the Navier-Stokes equations in three dimensions to determine the heat transfer and flow fields in an enclosure. While this particular CFD model has several options to deal with turbulent flows arising from fires, the specific turbulence model chosen for the present calculations is the k-ϵ model. Details of this turbulence model, including model constants, are found in appendix A.

The modeling technique used to simulate the gas flow is to divide the region of interest into a collection of small rectangular boxes or control volumes. The conditions in each control volume are initially ambient. Heat is then released in designated control volumes over time. The resulting flow or exchange of mass, momentum, and energy between control volumes is determined such that these three quantities are conserved. These fluid flow equations are expressed mathematically as a set of simultaneous, non-linear partial differential equations. After being discretized, the resulting finite volume equations are solved iteratively using a variant of Newton's method for computing coupled non-linear algebraic equations.

Approximately 34,000 control volumes were used to model each experiment. The sizes of the control volumes were varied using geometric progressions such that control volumes representing the fire and the space near the ceiling where thermocouples are located were of sufficient resolution to provide an adequate representation of the flow field. Symmetry planes were used to reduce the modeled space to one-quarter of the actual volume. At the walls, a no-slip boundary condition was used. This means that the flow velocities perpendicular and parallel to the wall were assumed to equal zero at the wall.

Convective energy losses from the gas to the ceiling were included in each calculation but the walls of the enclosure were assumed to be adiabatic. The ceiling was assumed to have the properties of steel. The assumption of adiabatic walls has a negligible effect on the calculations owing to the large space modeled and the distance that the fire was located from the walls. Radiation was included by assuming that 35 % of the fire's heat release rate was lost to the environment. The choice of 35 % was used to be consistent with the zone models.

3.3.2 NIST-LES

The large eddy approach to field modeling is an attempt to capture as much of the dynamic range of the fluid motion as possible consistent with a sufficiently fine spatial grid and an efficient flow-solving algorithm. Instead of relying on a turbulence model to time-average unresolvable convective motion, the large scale eddies are simulated directly and sub-grid scale motions are suppressed. If the computational grid is sufficiently fine relative to the characteristic length scales of the phenomena of interest, then the resolvable flow field is an adequate representation of the actual flow. The Reynolds number, a program input whose value depends on the grid resolution, is used to define an effective kinematic viscosity which represents dissipation on length scales below the resolution of the grid.

The transport of combustion products is calculated directly from a weakly compressible form of the Navier-Stokes equations. This approximation involves the filtering out of acoustic waves while allowing for large variations in temperature and density [23]. The fire itself is prescribed in a manner consistent with a mixture fraction based approach to combustion, but the detailed combustion chemistry is not simulated. Lagrangian particles representing burning fuel are introduced into the flow domain and collectively represent the fire. The level of complexity involved in prescribing the burning history of the fuel elements depends on the scenario of interest and the available spatial resolution.

The experiments modeled in this paper used a computational domain of 30.0 m by 22.0 m by 14.9 m. A uniform grid was used to perform the calculations for 500 kW and the 2.7 MW fires. The number of grids was 144 by 64 by 96 producing about 885,000 control volumes capable of resolving 0.15 m. The temperature at each location was calculated every 0.05 s and then averaged every 4 s to be consistent with the sampling rate of the data logger used to record the thermocouple measurements. Adiabatic boundary conditions were prescribed at the ceiling. The side boundaries of the domain were open and the ambient pressure was prescribed there.

The computations reported in this paper require approximately 25 microseconds per cell per time step on an IBM RS 6000/58H server, and use several hundred megabytes of memory. One distinct advantage of doing CFD modeling with high resolution and with the minimal use of turbulence models is that the computed smoke flow has a realistic appearance. An example of this is found in figure 2 where the simulated plume and smoke filled draft curtain is pictured. The smoke eddies shown in the computed plume structure resemble the observed plume structure of this particular experiment. Additional information concerning this model may be found in reference 25.

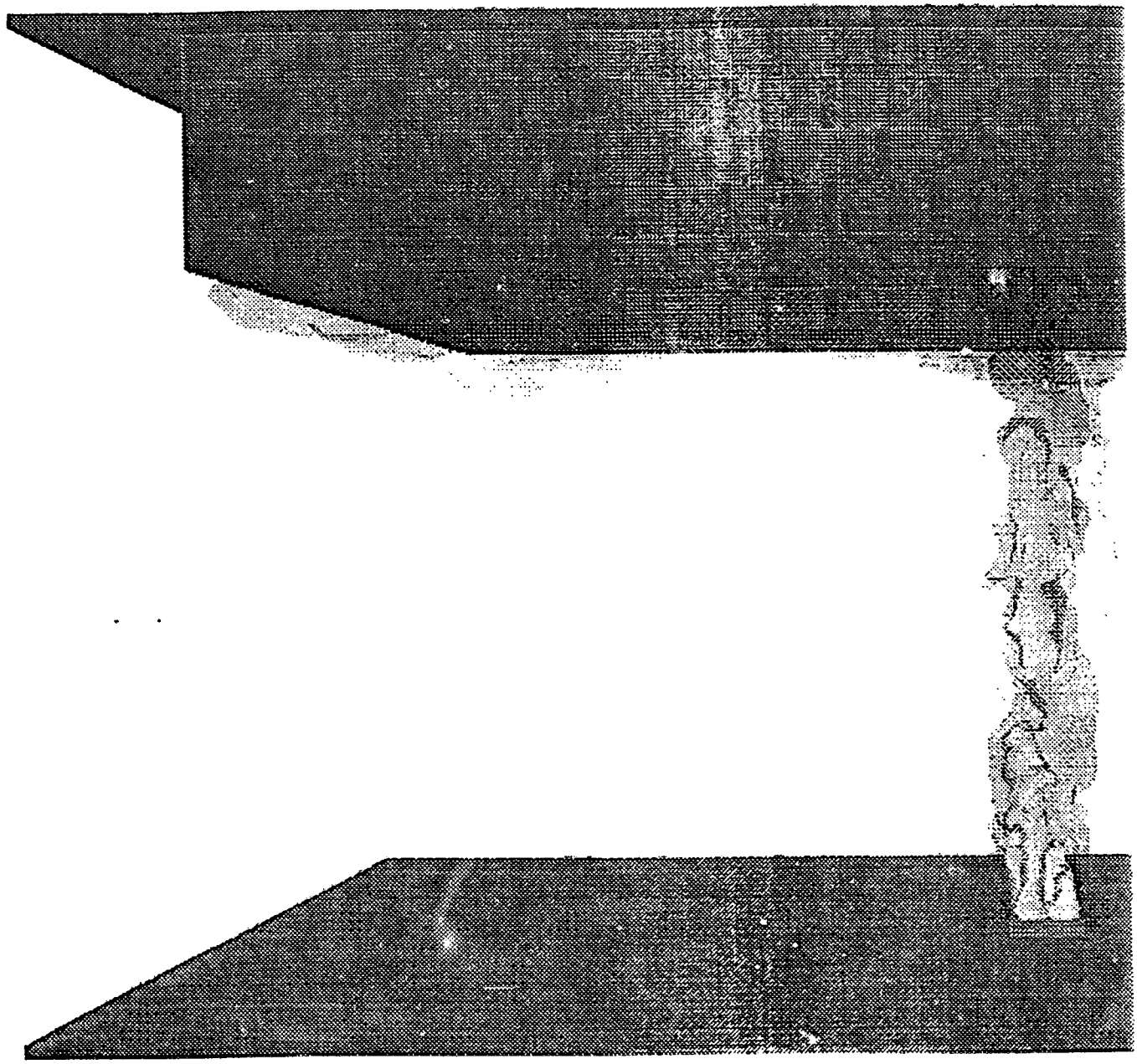

Figure 2 Smoke Movement Calculation in the 15 m Hangar using NIST-LES

4.0 Fire Model Performance

Fire models can be used to predict a variety of fire related phenomena including gas temperature, smoke and heat detector activation, gas and smoke movement, etc. In this section, a particular predictive capability of each model is compared against the equivalent measurement from the hangar experiments. In making these comparisons, the reader should continually keep in mind that experimental measurements contain uncertainties, and that comparisons to models are in agreement to the extent that the predictions lie within the uncertainties of the experimental measurements. Model predictions also have uncertainties associated with each value. One source of these uncertainties comes from using the experimentally measured heat release rate as a model input. A second source of uncertainty is the use of an assumed radiation fraction, or the fraction of the total energy radiated from the fire.. All models studied in this report use a constant radiative fraction to obtain the convective heat release rate for the fire, and deviations from this value will introduce uncertainty in the model results.

Other sources of uncertainty in the experiment which can cause deviations from the model predictions include air leaks in the hangar roof and walls and the impact of wind causing drafts within the structure. Experimental uncertainties in large scale fire experiments are difficult to determine accurately since individual tests do not allow the experimenter to assess reproducibility of the experimental results.

The accuracy of model predictions is also impacted by the choice of physical approximations used in the modeling and the numerical methods used to obtain a solution. Examples of physical approximations impacting the calculation would include heat transfer from the hot gas to the walls, the conduction of heat through the walls, the distribution of radiation from the fire to the surroundings, etc.. The choice of numerical methods is of particular importance for CFD models where the choice of grid resolution can, if done improperly, lead to substantial errors in the calculation.

Model comparisons are done at 75 s, 150 s, and 225 s after ignition. The rationale for the choice of these times is that 75 s was approximately when the temperature rise at the ceiling began to level off, and the other two times are spaced far enough apart to observe the slow heating of the gas and the impact of the growing hot layer on the ceiling jet as the fire approaches a steady state. Additional comparisons are made earlier in time depending on the particular model prediction to be tested.

4.1 Model inputs

Each of the fire models studied in this paper used a common set of initial and boundary conditions with a few exceptions which are noted below. The hangar was described in section 2.0. For the zone models, it was assumed that the ceiling was level and had a height of 14.9 m. The draft

curtain area of 24.4 m by 18.3 m was used to define the area of the fire compartment. The draft curtain was 3.7 m deep and was modeled either as a set of doors or as a draft curtain depending on the flexibility of the model. The heat release rate used for each test was based on a polynomial fit of the experimental data. The polynomial fits of the data from the load cell, namely mass versus time, are given in figures 3 and 4. These polynomial fits were used in the CFD models. A set of discrete values based on the polynomial fits was used for the zone models. These values are tabulated below.

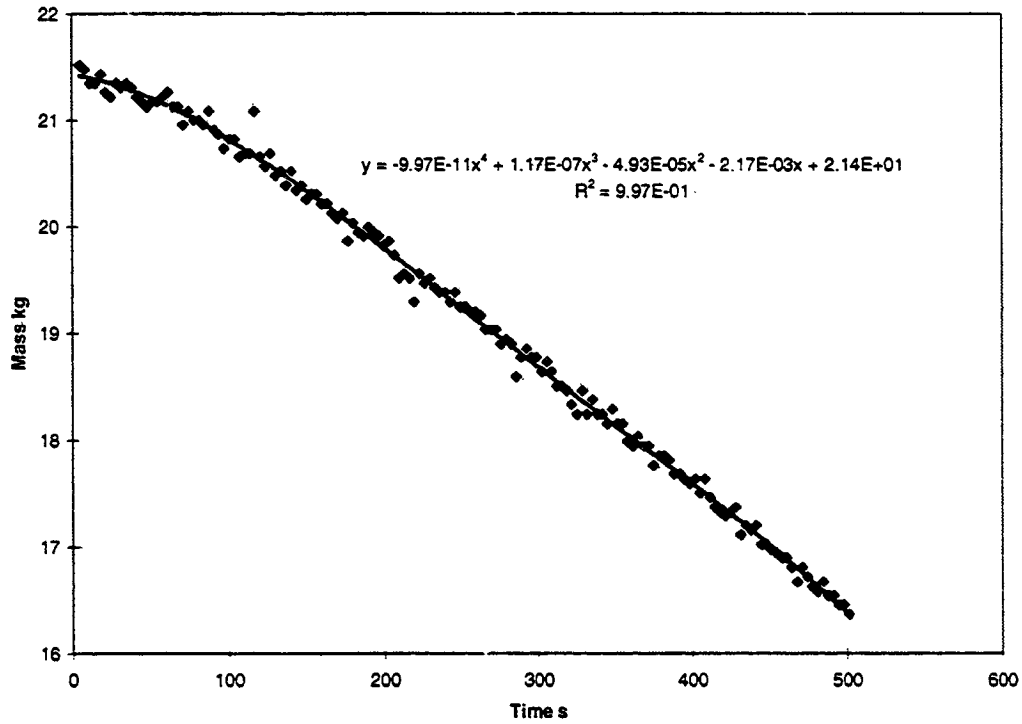

Figure 3 Load Cell Polynomial Fit for 500 kW Fire

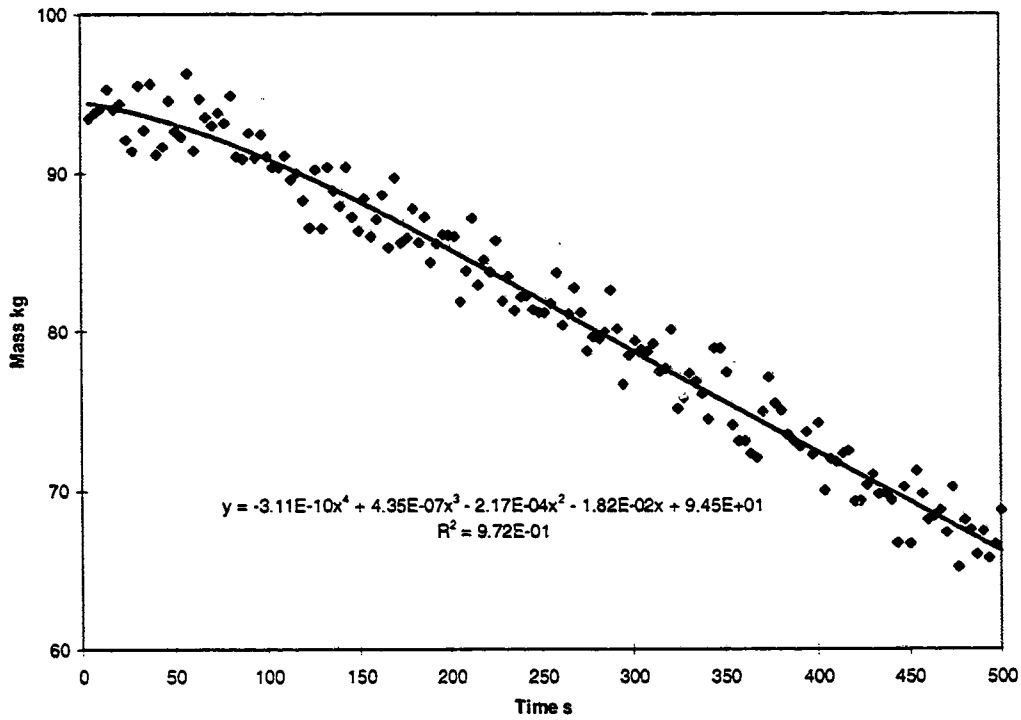

Figure 4 Load Cell Polynomial Fit for 2.7 MW Fire

Table 1: Heat release rates

Time s	500 kW fire kW	2.7 MW Fire kW
0.	0.	0.0
1.	99.	803.
10.	not used	965.
20.	174.	1135.
50.	273.	1582.
100.	388.	2139.
200.	481.	2693.
300.	478.	2766.

For the correlations which required only a single heat release rate at the times of comparison(i.e. 75 s, 150 s, and 225 s), the values used were 338 kW, 453 kW, and 485 kW for the 500 kW fire and 1888 kW, 2496 kW, and 2743 kW for the 2.7 MW fire.

A radiative fraction of 0.35 was used for each fire model. The radiative fraction represents the fraction of energy lost from the fire by radiation to the environment. For those models which could accommodate a conducting ceiling, steel (thermal conductivity of 60 W/m K, specific heat of 480 J/kg K, and density of 7850 kg/m^3) was used for the ceiling material. The plume correlations, Alpert's ceiling jet correlation and the atrium model in FPEtool do not allow the user to account for different ceiling materials. All the other computer models included the steel ceiling except NIST-LES where the ceiling was assumed adiabatic.

4.2 Centerline Plume Temperatures

The centerline plume temperature for each test was determined by comparing the temperatures at each thermocouple located at the geometric center and at radii of 1.5 m and 3.0 m from geometric center in the experimental north, south, east, and west directions. The temperature distribution from these measurements can be used to deduce where the plume center is located as a function of time. The maximum temperature recorded by this set of nine thermocouples is used as the plume centerline temperature. This value is either equal to or less than the true plume centerline temperature as one of the nine thermocouples would have to be positioned exactly at plume center at each measurement time to yield the true centerline plume temperature. The uncertainty interval expressed with each measurement includes not only the uncertainty based on the thermocouples but includes an estimate of uncertainty based on the spatial sparsity of the measurements. The important comparison is not the temperature but the temperature excess or

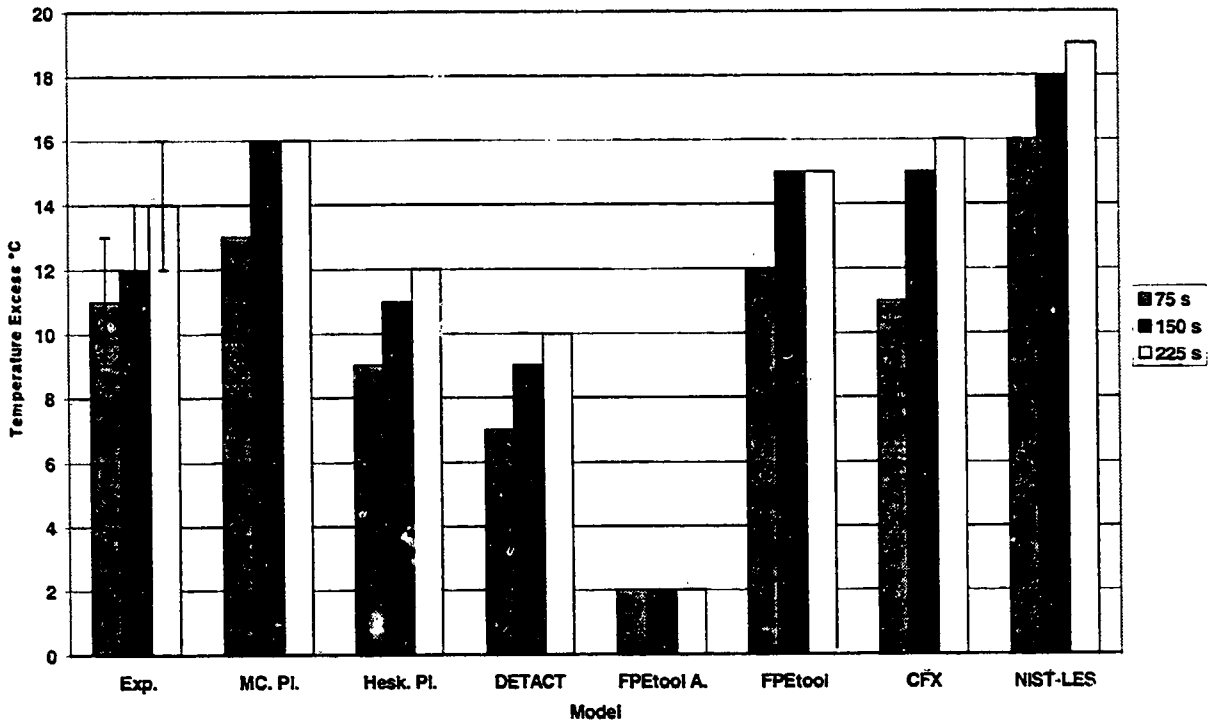

Figure 5 Plume Centerline Temperature Excess for the 500 kW Fire

rise above ambient. Figures 5 and 6 show the model predictions compared with the estimated excess centerline plume temperature for the three times of interest. The ambient temperature for the 500 kW fire was 28 °C and for the 2.7 MW fire it was 27 °C. (The uncertainty in the experimental data is given by the error bars.)

For the 500 kW fire, the model which performed most poorly was the atrium model in FPEtool, which predicted a 2 °C temperature excess. The NIST-LES model over predicted the temperature rise by about 45 %, DETACT under predicted the temperature rise by 30 %, while all the other model predictions were within the measurement uncertainty. Model predictions for CFAST and LAVENT were not given since neither model supports temperature predictions for $r/H < 0.2$.

For the 2.7 MW fire, the atrium model in FPEtool under predicted the temperature excess by about a factor of 3. The temperature excess for this test was about 40 °C. Other models which failed to predict temperatures within 25 % of the measured temperature excess include DETACT and NIST-LES.

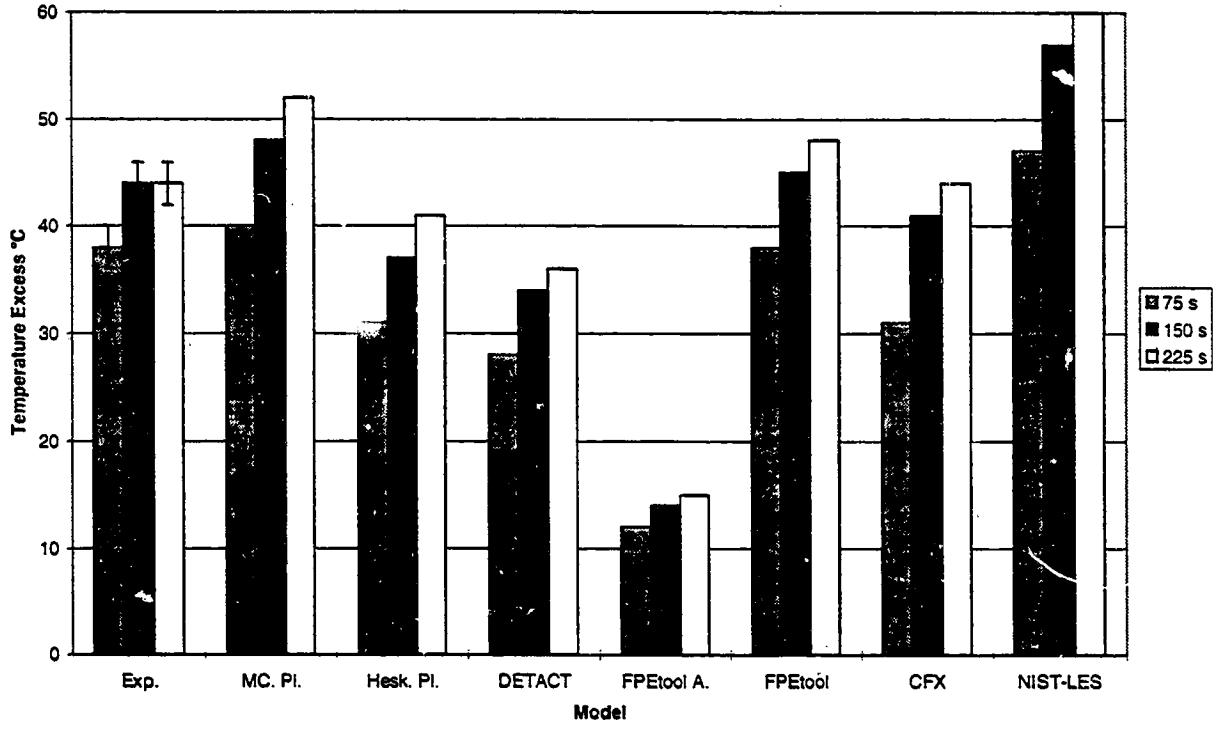

Figure 6 Plume Centerline Temperature Excess for the 2.7 MW Fire

4.3 Radial Temperatures From Plume Center

Radial temperature measurements were determined using thermocouples located 0.31 m beneath the ceiling at 1.5 m, 3.0 m, 6.1 m and 8.5 m from the center of the fire in the north and south directions and at 1.5 m, 3.0 m, 6.1 m, 9.1 m, and 11.6 m from fire center in the east and west directions. The roof had a slope of 3 degrees in the east and west directions with the roof sloping

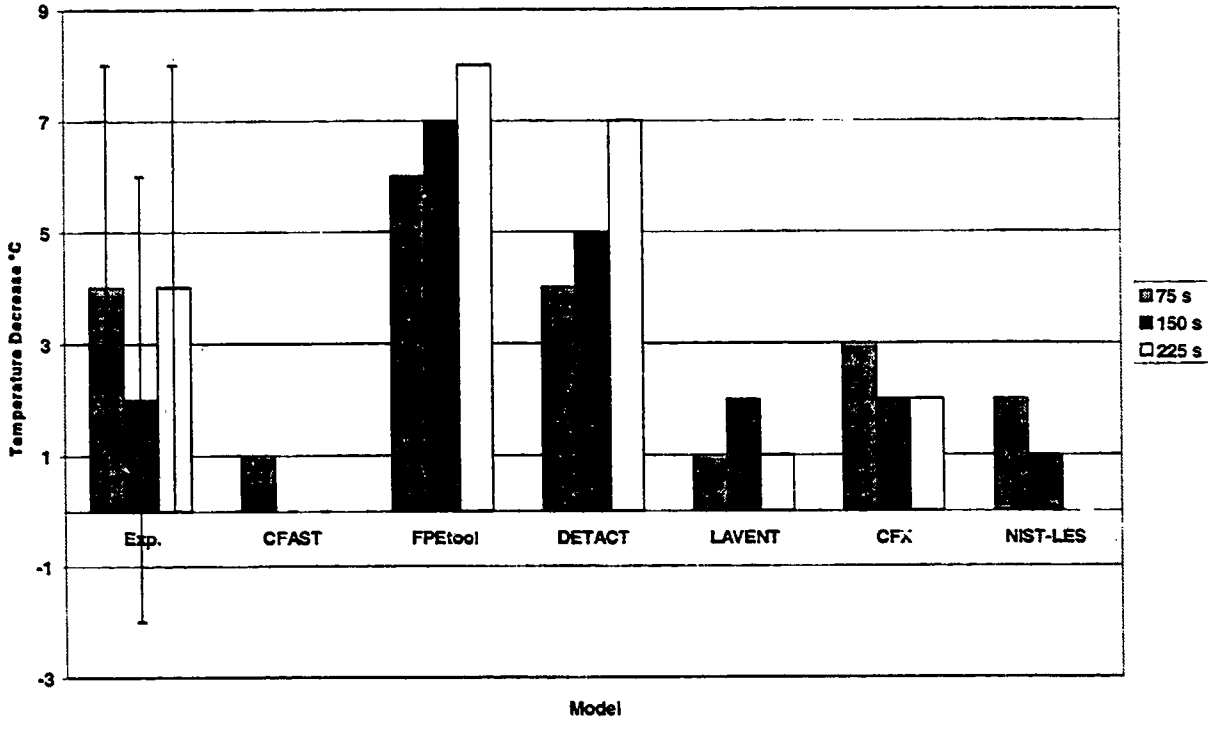

Figure 7 Radial Temperature Decrease Between 3.0 m and 8.5 m for the 500 kW Fire

up to the center of the hangar in the east direction and down toward the hangar wall in the west direction. Tables 1 - 6 in appendix B list the radial temperature measurements for the 500 kW and 2.7 MW tests and the computer model predictions for CFAST, DETACT, FPEtool, LAVENT, CFX, and NIST- LES. While the peak temperature usually does not occur at exactly the geometric center due to movement of the plume, the peak temperature usually occurs within 1.5 m of the center for both of these tests. The experimental values in the north-south and east-west directions represent averages of pairs of thermocouples in each direction. The distance to the draft curtain from fire center was 12.2 m in the east and west directions and 9.1 m in the north and south directions.

For the 500 kW fire, all the models gave predictions which were either within experimental uncertainty or close to the experimental uncertainty. For the 2.7 MW fire, CFAST over predicted the temperature rise by as much as 100 % for radial distances 9.1 m from the fire. Other models which over-predicted the temperature rise by more than 25 % included FPEtool (fire simulator), LAVENT, and NIST-LES. DETACT under-predicted the temperature rise by more than 25%. DETACT does not include any layer interaction with the ceiling jet which may

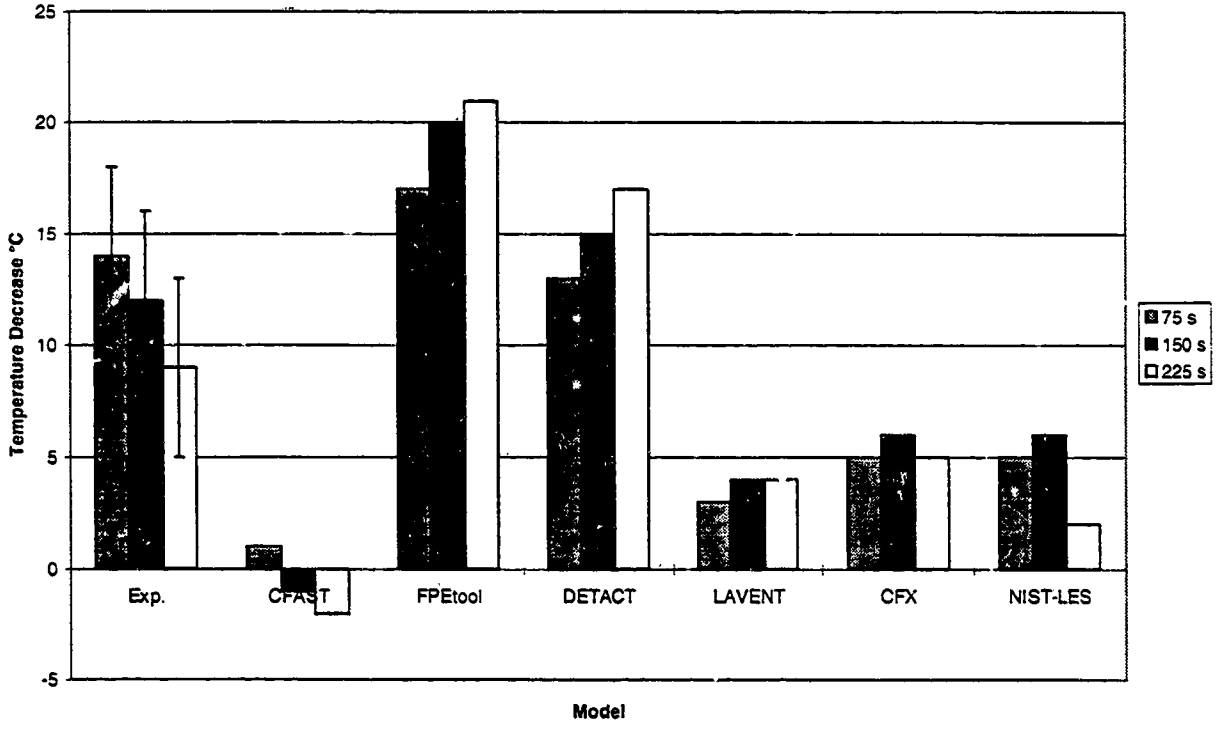

Figure 8 Radial Temperature Decrease Between 3.0 m and 8.5 m for the 2.7 MW Fire

account for part of this correlations under prediction of temperature.

A comparison of the predicted temperature decrease along the ceiling jet from a distance 3.0 m from plume center to 8.5 m from plume center offers another way of looking at the accuracy of ceiling jet models. At 3.0 m, r/H = 0.2 which is the closest measurement location to fire center where the ceiling jet correlations are valid and 8.5 m represents the largest radial distance from the fire center in the north - south direction before the draft curtain is encountered. This region was entirely out of the plume and provides a measure of each model's temperature dependence outside the plume. Figure 7 gives a comparison for the 500 kW fire of the temperature difference between 3.0 m and 8.5 m radially out from plume center for both the models and the experiments.

The experimental difference was obtained by averaging the temperature difference in all four directions. Figure 8 provides the same differences for the 2.7 MW fire with the experimental values representing averages in the east and west directions only.

The impact of the layer on the radial temperature difference can be seen by observing that as the layer continues to grow, the temperature difference decreases for the 2.7 MW fire as shown in Figure 8. For the 500 kW fire, the effect is not evident (see Figure 7) since for this fire the layer temperature is much closer to the ambient temperature.

For the 500 kW fire, all models provide predictions which lie within the experimental uncertainty. For the 2.7 MW fire, CFAST predicted a slight increase rather than the measured decrease in temperature for the measurements at 150 s and 225 s. The models LAVENT, CFX, and NIST-LES all predicted smaller temperature decreases than were measured. FPEtool and DETACT predicted temperature decreases at 75 s which were within experimental uncertainty, but by 225 s, the predicted decreases were larger than the measured decreases. DETACT does not include a hot layer and so would not be expected to follow the trend to a more isothermal ceiling jet as the hot layer develops. FPEtool is also not following this trend even though the model does include a hot layer interaction.

4.4 Ceiling Jet Temperature Profile

The variation of ceiling jet temperature with respect to distance beneath the ceiling was measured using five thermocouple trees. Four of the trees were located at 6.1 m in the north, south, east, and west directions from geometric center and the fifth tree was located at 9.1 m from geometric center in the east direction. Each tree contained five thermocouples located 0.15 m, 0.31 m, 0.46 m, 0.61 m, and 0.76 m beneath the ceiling.

Ceiling geometry which could produce significant deviations from smooth ceiling predictions included 0.25 m I-beams running in the north-south direction and spaced every 4.1 m on center. The fires were positioned half way between two of these beams which meant that the ceiling jet flow in the east and west directions encountered one of these beams at 2.05 m and again just after the thermocouple trees at 6.15 m. The I-beams supported a corrugated metal roof which was covered with tar and gravel. The I beams were supported from below by trusses running east-west which were spaced every 6.1 m. Flow in the north-south directions would encounter one of these trusses at 3.05 m from geometric center.

The experimental data are presented in tables 7 and 8 in appendix B for the two tests. In general, the temperature is approximately constant over the measured distance at all radial positions. Exceptions occur for the south and west thermocouples of the 2.7 MW fire where the temperature 0.15 m beneath the ceiling is lower than those measured by the other thermocouples on these trees. The same constant temperature profile exists for these thermocouples below 0.31 m. The r/H ratios for these measurements are 0.41 for the 6.1 m thermocouple trees and 0.61 for

the 9.1 m tree.

The model predictions are presented in tables 9 - 12 in appendix B. The models which provide temperature as a function of distance beneath the ceiling are LAVENT, CFAST, CFX, and NIST-LES. For the 500 kW fire, the temperature remained approximately constant from 0.15 m below the ceiling to 0.76 m below the ceiling 6.1 m radially from the fire center for all four directions. The same constant temperature profile was noted at 9.1 m from fire center in the east direction. The fire model LAVENT predicted a 0 °C to 3 °C decrease, CFX at most a 1 °C decrease, NIST-LES a 3 °C decrease while CFAST predicted a 3 °C to a 6 °C decrease at 6.1 m. At 9.1 m, all the models except NIST-LES predicted temperature changes of no more than 1 °C. NIST-LES predicted a 3 °C decrease.

For the 2.7 MW fire, at 6.1 m from fire center, the temperature remains fairly constant from 0.3 m to 0.76 m below the ceiling with the thermocouple positions at 0.15 m registering a substantially lower temperature in the south and west. In comparison, CFAST predicted a decrease in temperature between 0.15 m and 0.76 m at a distance of 6.1 m to be 14 °C to 18 °C, LAVENT predicted a decrease of 8 °C, CFX predicted at most a decrease of 1 °C, and NIST-LES predicted a decrease of 4 °C to 5 °C. At 9.1 m, CFAST predicted a temperature increases of 4 °C to 6 °C between 0.15 m and 0.3 m followed by a decrease of 6 °C to 9 °C between 0.3 m and 0.76 m, NIST-LES predicted a temperature decrease of 4 °C to 6 °C while LAVENT predicted a temperature increase of 2 °C to 4 °C between 0.15 m and 0.3 m followed by a decrease of 3 °C between 0.3 m and 0.76 m and CFX predicted temperature changes of no more than 1 °C.

4.5 Ceiling Jet Velocity

Ceiling jet velocity was measured using two Sierra Steel-Trak Industrial Insertion Mass Flow Meters (series 640). These meters were positioned 6.1 m from the geometric center to the north and east direction and were located 0.3 m beneath the ceiling. The mass flow meter contains two sensors, a velocity sensor and a temperature sensor to compensate for temperature changes. Internal circuitry heats the velocity sensor above ambient with respect to the temperature sensor and measures the cooling effect of the gas flow.

Figures 9 and 10 present a comparison of the experimentally measured gas flow with the predictions of CFAST, DETACT-QS, FPEtool (Fire Simulator), LAVENT, CFX, and NIST-LES. The uncertainty values listed with the experimental measurements represent measurement

error in the mass flow meters based on the manufacturers calibration tests.

For the 500 kW fire, the measured ceiling jet velocities are 0.2 m/s to 0.3 m/s lower in the north direction than in the east direction. Since the probes are directional, a slight misalignment of the probes with flow velocity may be responsible for this difference in flow velocities. The models CFAST, DETACT-QS and LAVENT predict flow velocities that are consistently high by 50 % or more from the measured velocities. FPEtool provided predictions which ranged from 25 % to more than 50 % higher than the measured values. The CFD models provided predictions within 25 % of the measured values with the exception of NIST-LES at 75 s where the model over-predicted the velocity by more than 50 %.

For The 2.7 MW fire, the measured flow velocities in the north direction increase as expected

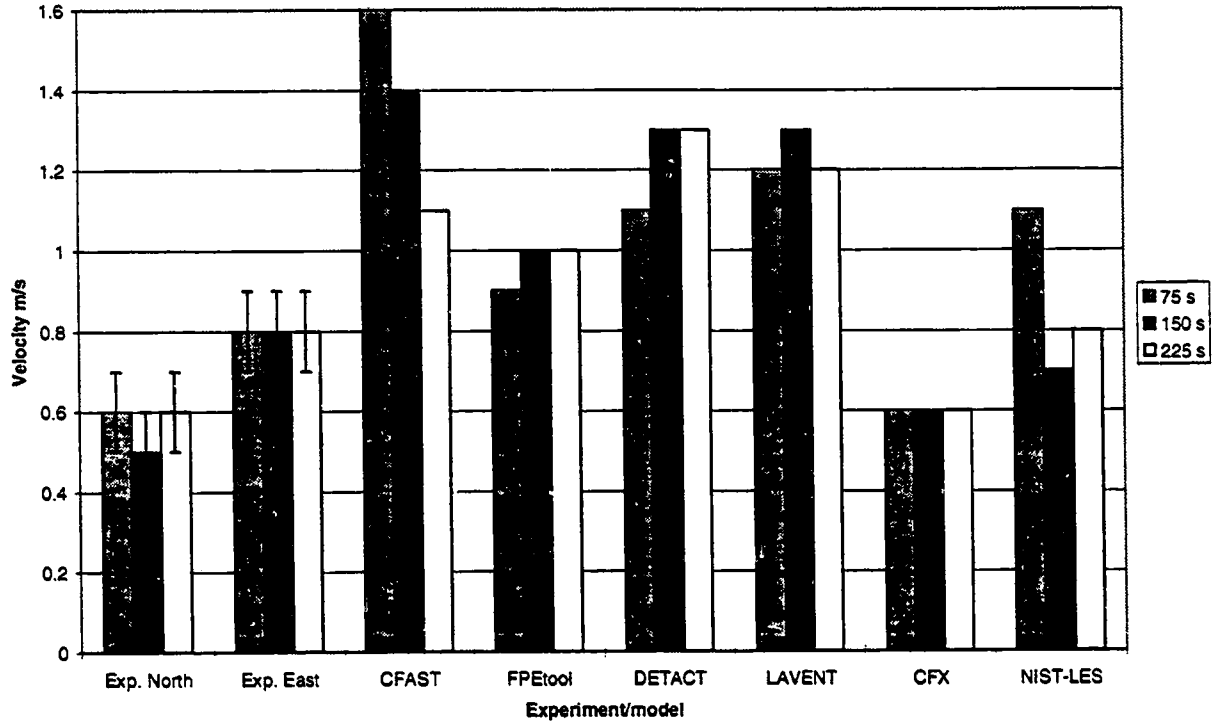

Figure 9 Ceiling Jet Velocity at 6.1 m for the 500 kW Fire

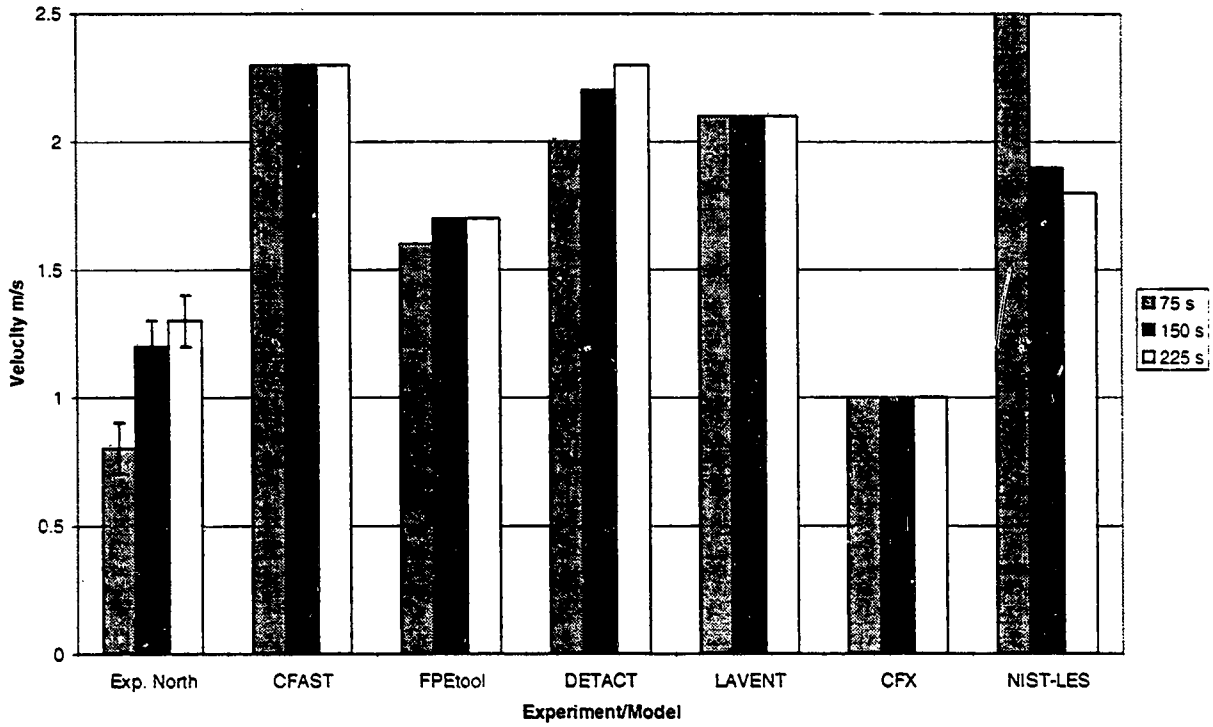

Figure 10 Ceiling Jet Velocity at 6.1 m for the 2.7 MW Fire

with the increased heat release rate. The measured flow velocities in the east direction decrease to very low values suggesting that the velocity probe may not have worked properly for this test. Comparing only the north data with the models, CFAST, DETACT-QS, LAVENT, and NIST-LES predict flow velocities which are 50 % or more higher than the measured flow velocities. FPEtool predicts velocities which are 30 % to more than 50 % higher than the measured values. CFX predicted flow velocities that are within 25 % of the measured values.

4.6 Draft Curtain Filling Time

Draft curtain filling time provides a measure of the entrainment by the plume in each of the fire models used. The draft curtain for these experiments was 24.4 m by 18.3 m and was 3.7 m deep. Experimental filling times were determined using the thermocouple located at 9.1 m to the east of geometric center and 3.0 m below the ceiling. This thermocouple was positioned within 0.61 m of the bottom of the draft curtain and provided a comparison time for the hot gases reaching this

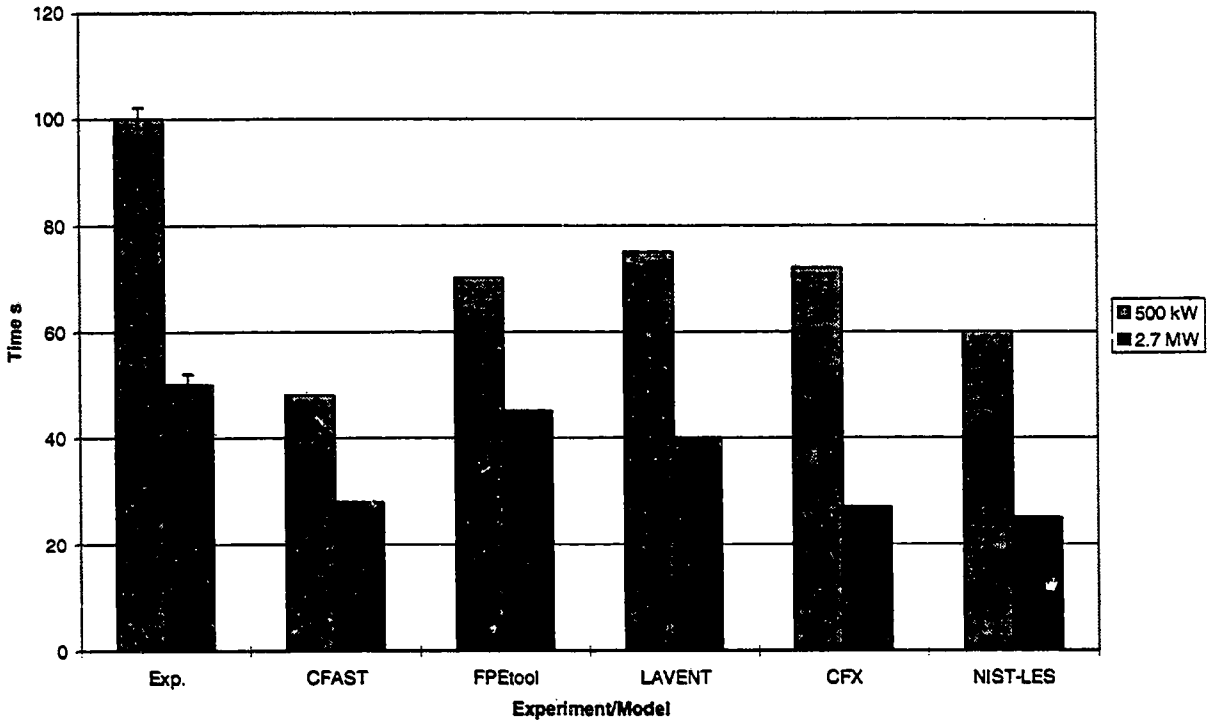

Figure 11 Draft Curtain Filling Time

depth within the draft curtain. Figure 11 presents a comparison of the experimentally measured filling time with the times predicted by the fire models. A temperature increase of 0.5 °C was used to indicate the arrival of the hot gas at a given location. All models under predicted the filling times with the 500 kW test being most poorly represented. This discrepancy in predicted measured fill times would be expected since visual observations indicated that smoke was able to flow under the draft curtain prior to the curtain filling with smoke.

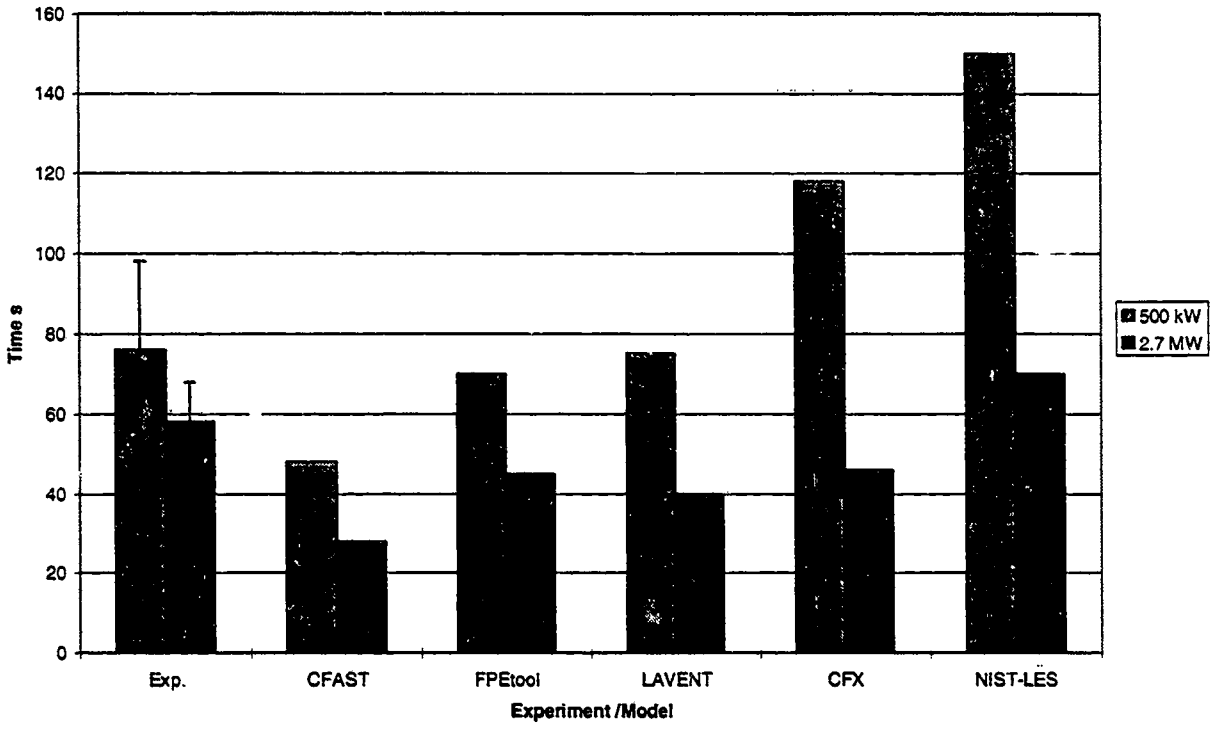

Figure 12 Draft Curtain Spilling Time

4.7 Draft Curtain Spilling Time

Thermocouples located at 11.6 m in the north and south directions and 14.6 m in the east and west directions from geometric fire center were available to determine when hot gases began flowing outside the draft curtains. Each of these thermocouples were located 0.3 m below the ceiling and 2.4 m outside the draft curtain. The north thermocouple was located in a skylight which could have increased the response time for this thermocouple. The spill times reported in

figure 12 are based on a 0.5 °C temperature rise for each thermocouple. The uncertainties listed with the measurements are based on the sampling rate of approximately 4 s per scan. Since the thermocouples located are 2.4 m beyond the draft curtains, the measured spill times include the time required for the hot gas to rise up along the draft curtains to the ceiling and move the additional 2.4 m to reach the thermocouple. Typical ceiling jet velocities are on the order of 1 m/s or less, hence the measurements may overestimate the spill time by 5 s to 10 s.

The location of the plume center can impact the spill times as a function of distance if the plume leans preferentially in one particular direction. Measurements, using thermocouple temperatures, indicate that the location of the plume center early in the 500 kW fire was 1.5 m [illegible]th of geometric center while for the 2.7 MW fire, the plume center was located 1.0 m to the southeast of geometric center.

For the zone models, the spill time occurs when the hot gas fills the draft curtain volume. The CFD models include momentum and indications from the experiments are that the hot gas flows out of the curtained volume prior to the curtained volume filling with hot gas. The reason why the hot gas spills under the draft curtain before the curtain fills is that the draft curtain is not sufficiently deep for the buoyant force to stop the downward motion of the hot gas before the edge of the draft curtain is reached. A comparison of the predicted spill times of the fire models with the experimental average of the spill time over the four directions is given in the figure 12. The uncertainties given with the experimental averages represent the one sigma confidence interval. For the 500 kW fire, FPEtool and LAVENT provided predictions within the experimental uncertainty while the two CFD models over predicted the spill time by more than 50 % and CFAST under predicted the spill time by more than 25%. For the 2.7 MW fire, CFAST and LAVENT provided predictions within 50 % of the measured values while FPEtool, CFX, and NIST-LES provided predictions within 25 % of the experimental values.

4.8 Temperature Change across Draft Curtain

As the hot gas flows under the draft curtain, additional entrainment should cool the hot gas as it moves into the adjacent ceiling volumes. Using the east and west thermocouples at 11.6 m which is 0.61 m inside the draft curtain and the east and west thermocouples at 14.6 m which is 2.4 m outside the draft curtain, an average inside - outside temperature difference can be calculated in the east-west direction. In the north-south directions, thermocouples located at 8.5 m and 11.6 m are averaged to provide the equivalent inside-outside temperature difference in this direction. These measurements are used to determine how each model handles the additional entrainment associated with the flow of the hot gas under the draft curtains. Figures 13 and 14 present a comparison of the predicted temperature difference for each model compared with the measured temperature difference. None of the zone models support a ceiling jet algorithm in a room adjacent to the fire room. Only the CFD models presently are able to model this flow. For the 500 kW fire, NIST-LES gave predictions within experimental uncertainty for the N - S direction

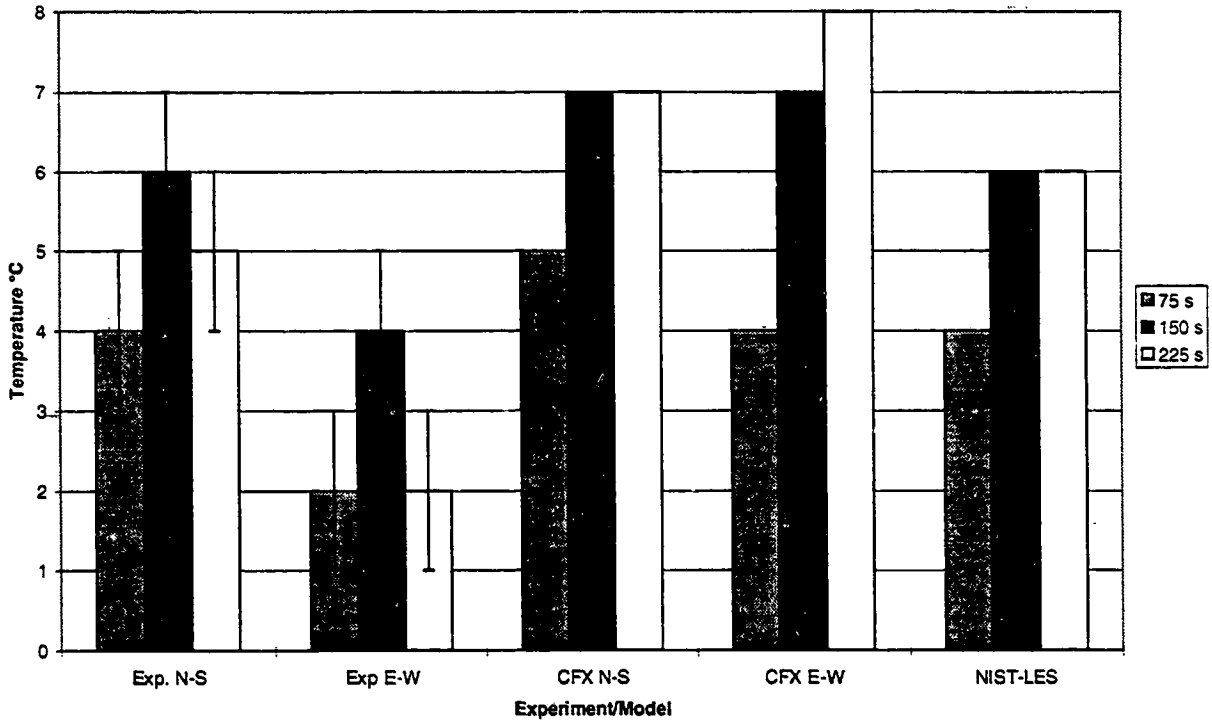

Figure 13 Temperature Difference Across Draft Curtain for the 500 kW Fire

while CFX gave comparisons that were either within experimental uncertainty or within 50 % of the measured value. Both models over predicted the temperature difference in the E - W direction. For the 2.7 MW fire, CFX under predicted the N - S temperature difference and over predicted the E - W temperature difference. NIST-LES also over predicted the E - W direction and under predicted the N - S temperature difference.

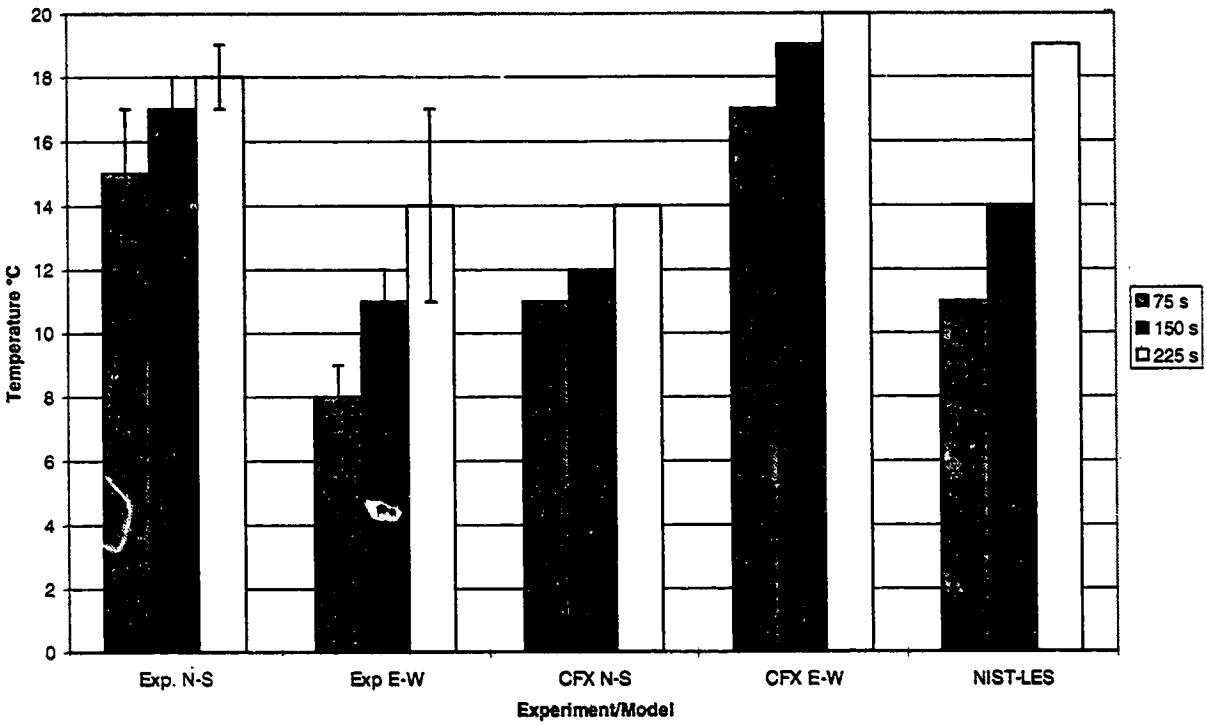

Figure 14 Temperature Difference Across Draft Curtain for the 2.7 MW Fire

4.9 Smoke Detector Activation

The activation of smoke detectors is handled by CFAST as a temperature criterion. The user has the option to set a specified target temperature which when reached would signify the activation of a smoke detector. The default value for smoke detector activation in this model is 11 °C above ambient [9]. The temperature calculated by the model in the fire room is based on the ceiling jet algorithm and so is not applicable for $r/H < 0.2$. In adjacent rooms or spaces, the layer temperature is used to predict smoke detector activation.

In FPEtool, a temperature criterion is used for smoke detector activation. The default value for smoke detector activation in this model is a temperature rise of 13 °C above ambient [24] and this value was used in the comparison with the experiments. The equations used to calculate the smoke detector's temperature rise are the same ones that are used for the heat detectors. To predict the smoke detector activation, the RTI in these equations is set to a small value to eliminate thermal lag.

In LAVENT, smoke detector activation is handled in a similar fashion to FPEtool. The fusible link algorithm is used with a very small RTI value such that there is no thermal lag.

Two issues must be addressed in this section. The first issue is the temperature criterion used to determine activation of smoke detectors at these heights. The second issue is how the models perform with their default values for smoke detector activation. The photoelectric smoke detectors were analog addressable spot type detectors which operate based on light scattering from smoke particles. Each detector contained a pulsed LED and silicone photo diode receiver which detects scattered light. The sensitivity setting for each detector for these experiments was 8.2 % per meter (2.5 % per foot).

Tables 13 and 14 in appendix B present the time to activation and the temperature rise recorded by a thermocouple adjacent to each smoke detector.

To compare the zone model predictions to the experimental data, the activation times in the four directions are averaged for each radius. The models were run for each radius and the results are presented in Figure 15 and 16. The reported deviations for the experimental results were

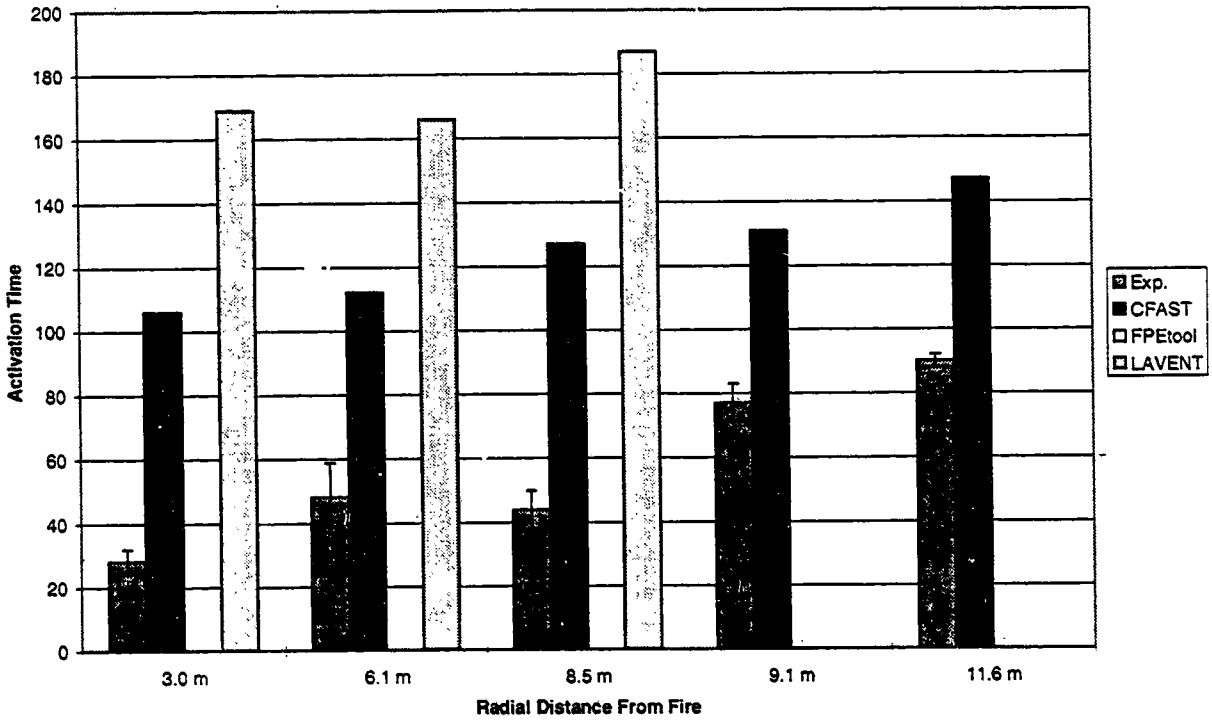

Figure 15 Smoke Detector Activation with Zone Model Predictions for the 500 kW Fire

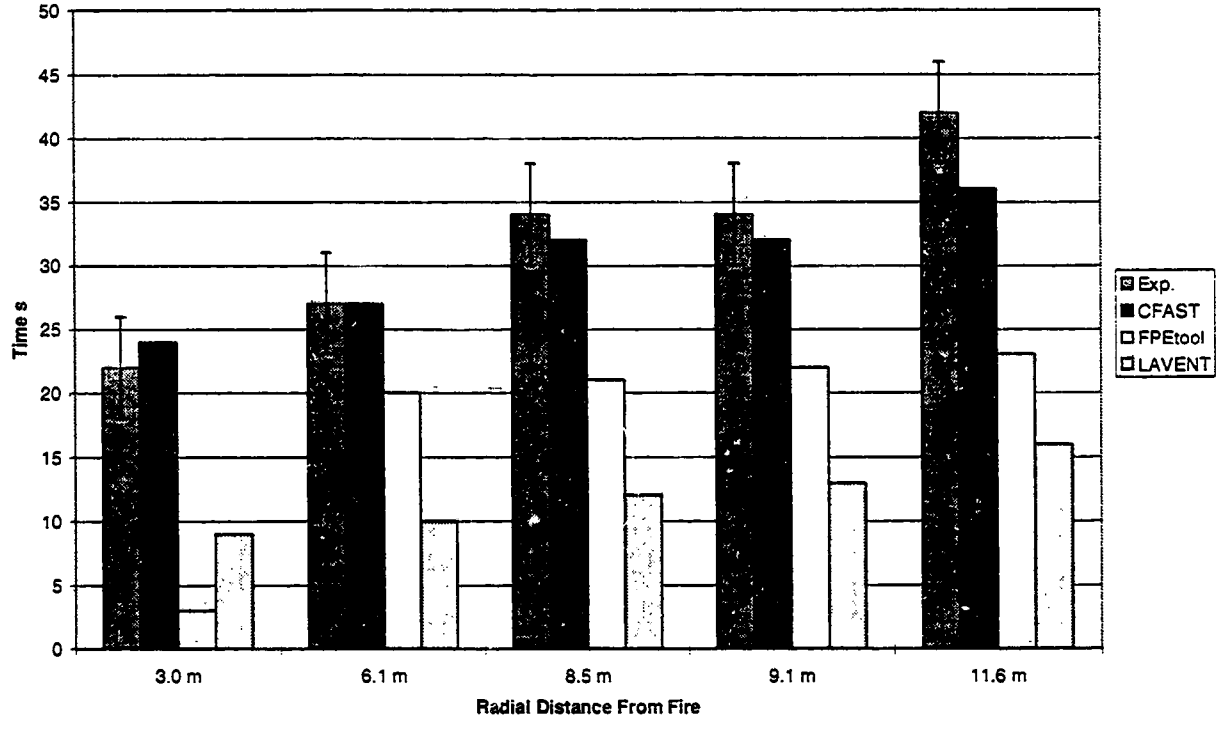

Figure 16 Smoke Detector Activation with Zone Model Predictions for the 2.7 MW Fire

determined by doing a least squares average of the two or four data points at a given radial distance from the fire. Additional error will occur due to the finite data sampling interval of 4 seconds. In figure 15, FPEtool and LAVENT did not predict smoke detector activation at all radial positions. The lack of activation is shown by no activation time being reported.

Comparisons of smoke detector activations must take into account the time required for the smoke from the plume to reach the detector. Zone models typically do not include these transit time effects and under predict the activation times for smoke detectors located at substantial distances from the fire.

The average temperature required to cause a smoke detector to go into alarm at 3.0 m and 6.1 m from fire center was 5 ± 2 °C for the 500 kW fire and 3 ± 3 °C for the 2.7 MW fire. For radial distances between 8.5 m and 11.6 m, the temperature required for a smoke detector to go into alarm was 3 ± 1 °C for the 500 kW fire and 2 ± 1 °C for the 2.7 MW fire. These values are significantly lower than the default values of 11 °C and 13 °C used in the zone models. Use of these lower values would improve the predictive capabilities of CFAST, FPEtool and LAVENT for the 500 kW fire. For the 2.7 MW fire, where the temperature rises quickly at the ceiling, the most important improvement would be to include the time of flight for the smoke to reach the detector in each model.

5.0 Summary

Figures 17 through 20 below summarize some of the comparisons that were made between the fire models and the fire experiments. The percentages shown in the bar graphs were determined by calculating the percentage difference between each experimental result and model prediction, discarding the best and worst comparison, and averaging the remaining comparisons. There were two instances, the radial temperature decrease and the temperature decrease across the draft curtain, where only the comparisons with the 2.7 MW fire were used since the 500 kW fire produced small numbers coupled with a relatively large experimental error. In these cases, all measurement comparisons were used to determine the percentage. Some models do not provide a predictive capability for a particular experimental measurement and are not included in the figure for that measurement. Temperature comparisons are based on the difference between the calculated and experimentally measured temperature rise above ambient.

A number of observations can be made concerning the comparison of the model results with the experimental measurements. For the plume centerline temperature, almost all of the models provided good predictive results. The notable exception was the atrium model in FPEtool which consistently predicted low temperature excesses. For the zone models, the prediction of the ceiling jet temperature as a function of distance from plume center was not particularly good using either the Alpert correlation or the Cooper correlation. The temperature dependence as a function of distance beneath the ceiling using CFAST was not observed in the experiment. A possible reason for this is that both correlations were based on smooth ceiling experiments. When ceiling beams are present, the possibility of producing substantial gas mixing can eliminate the

temperature stratification expected for a smooth ceiling. In addition, Alpert's correlation does not take into account a growing upper layer or allow for specific ceiling materials. Both the presence of the upper layer and the dependence that heat loss to the ceiling has on ceiling material should impact the temperature distribution in the ceiling jet. Ceiling jet velocity comparisons could also have been affected by the ceiling beams which would tend to reduce the speed of the smoke and hot gas due to interactions with the beams. This effect may explain why many of the zone models over predicted the ceiling jet velocity at the ceiling. FPEtool and LAVENT predicted the time for draft curtain filling and spilling to within 25% of the measured value. These two measurements are most sensitive to plume entrainment which suggests that the entrainment algorithms used in these models are acceptable at these heights.

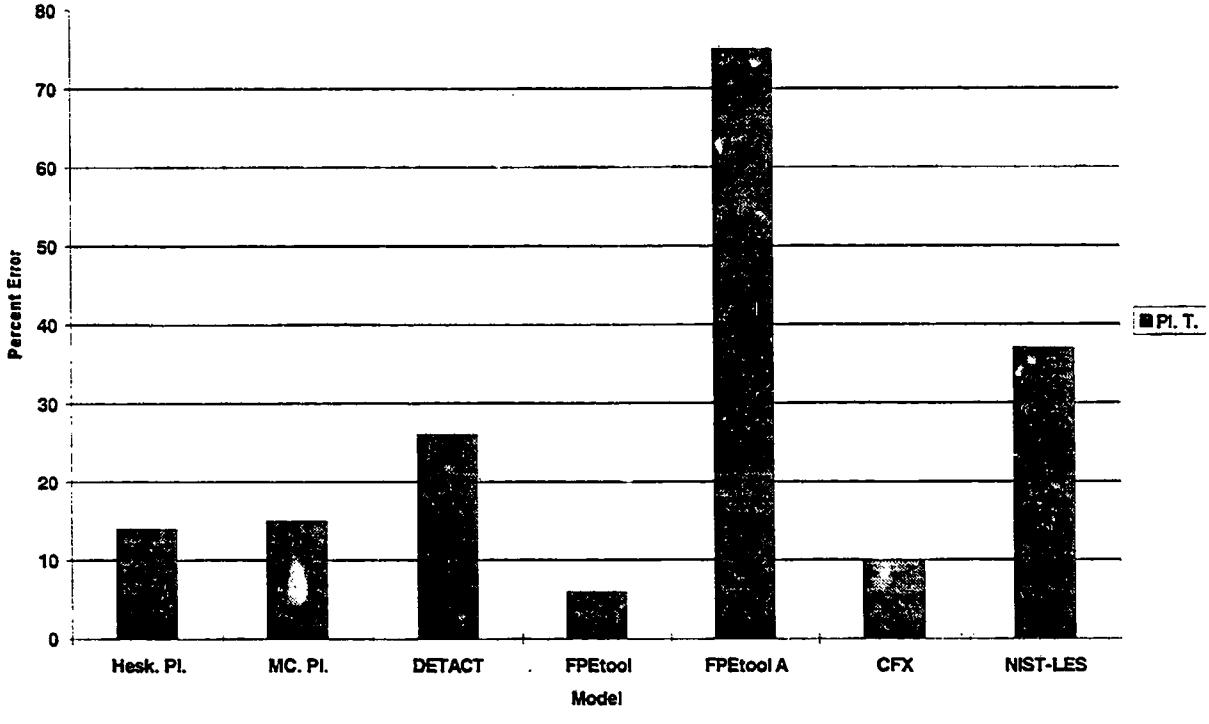

Figure 17 Deviations between Model Predictions and Measured Plume Centerline Temperature

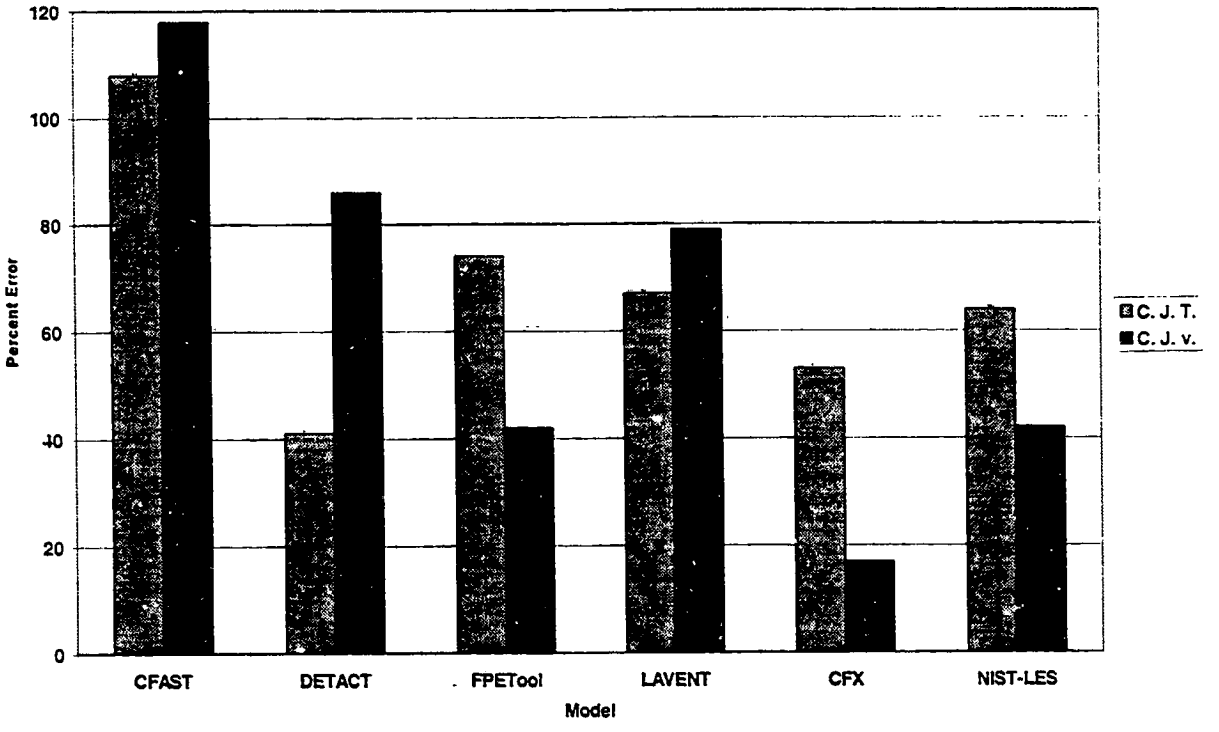

Figure 18 Deviations between Model Predictions and Measured Ceiling Jet Temperature and Velocity

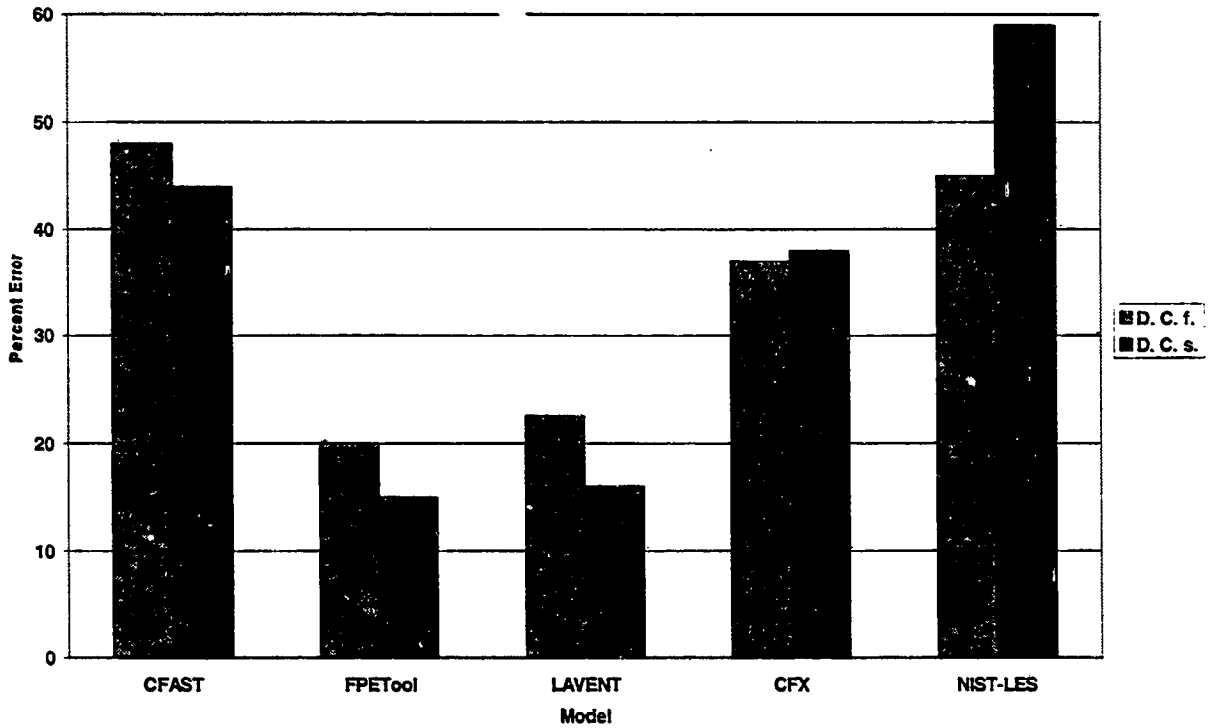

Figure 19 Deviations between Model Predictions and Measured Draft Curtain Filling and Spilling time

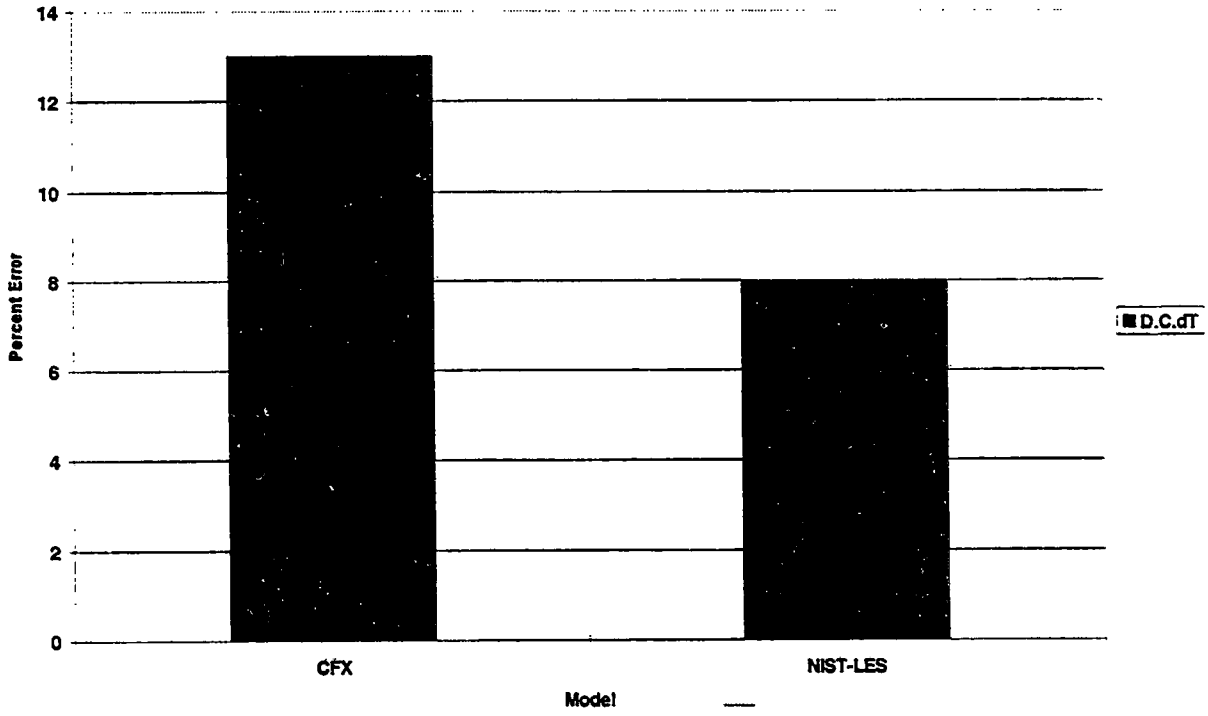

Figure 20 Deviations between Model Predictions and Measured temperature Jump Across the Draft Curtain

For the CFD model, CFX, good predictions of plume centerline temperature were expected since the turbulence constants used for the model were chosen to produce results in close agreement with the Heskestad plume model. This model also gave reasonable results for a number of other comparisons but the ceiling jet temperature decrease as a function of distance beyond plume center was not well represented by the model. This may be due to the finite number of computational volumes chosen to model the experiment where the resolution may not have been sufficient to track the temperature radially. The choice of turbulence constants may also have been at fault as the choice of the constants were based on plume correlations and not on ceiling jet correlations.

A comparison of the NIST-LES results with the experimentally measured temperatures show the model results over predict the temperatures for the tests considered here. The reason for the over prediction may lie in the spatial resolution. It has been observed that the model produces good agreement with empirical plume correlations when the spatial grid in the vicinity of the fire is about one tenth of the characteristic fire diameter

$$D^* = [\dot{Q}/(\rho_\infty T_\infty c_p g^{1/2})]^{2/5}$$

For the 500 kW and 2.7 MW fires, the characteristic fire diameters were 0.7 m and 1.4 m respectively, while the spatial resolution in both cases was about 0.15 m. The model works best when the fire is large enough relative to the overall enclosure so that the entrainment process can be captured directly without resorting to an empirical turbulence model. The fire size in the 2.7 MW test is approaching the point where the technique can be used, but there is still some relevant mixing that is not being resolved, leading to higher temperatures in the plume. The grid could have been refined to capture more of the mixing, but the particular model used at NIST is being designed to handle a large, spreading fire in a large space, and hence the grids are designed to provide reasonable resolution over the entire space, not just in a fraction of the space.

6.0 Conclusion

This study has attempted to provide a quantitative comparison of the predictions from several fire models with two well documented fire experiments conducted in a large hangar with a ceiling height of 14.9 m. Of the eight different comparisons made, the prediction of the plume centerline temperature was within 20 % for four of the seven models having this predictive capability. The atrium model of FPEtool was the only model to miss the measured temperature by more than 50% which indicates that this model should not be used at these heights. The model predictions of radial temperature variation and ceiling jet velocity were much less satisfactory which suggests that work still remains to be done in these areas. Model predictions of temperature variation as a function of depth beneath the ceiling provided a poor comparison with the experimental data. It is suspected that mixing caused by the ceiling beams may eliminate the expected temperature stratification observed in smooth ceiling experiments. The performance of the CFD models in some comparisons is better than the zone models but in other comparisons no advantage was gained by using the CFD models over the zone models.

The prediction of smoke detector activation was particularly bad. The default criteria of 11 °C or 13 °C temperature increases are too large by about a factor of two at this height for both the 500 kW and 2.7 MW fires. The smoke detector activation models need to be revised in order to include a dependence on height above the fire and distance from the fire centerline.

It is important to recognize that models which performed poorly in this study may provide good predictive capabilities at substantially different ceiling heights, enclosure sizes, or in structures where the ceiling surface is smooth. The study is based on only two fire tests and uses only a single fuel. Hence, models which have performed well in these tests may not perform as well at these heights when the fuel type or building geometry deviates significantly from the present test parameters. For each model application, the reader is encouraged to seek out the appropriate validation studies and not judge a fire model on a single set of experiments. Of prime importance

is to ensure that the model used contains the proper physics to handle the desired application. A model which may give good results in a validation study may fail when applied to a situation where the physics in the model is inappropriate for the application.

References

[1] Gott, J., Lowe, D., Notarianni, K. A., and Davis, W. D., "Analysis of High Bay Hangar Facilities for Detector Sensitivity and Placement", National Institute of Standards and Technology, Special Publication, To Be Published.

[2] Walton, W. D., and Notarianni, K. A., "A comparison of Ceiling Jet Temperatures Measured in an Aircraft Hangar Test Fire with Temperatures Predicted by the DETACT-QS and LAVENT Computer Models", National Institute of Standards and Technology, NISTIR 4947, 1992.

[3] Duong, Duy Q., "The Accuracy of Computer Fire Models: Some Comparisons with Experimental Data from Australia", *Fire Safety Journal* 16 (1990) 415-431.

[4] Notarianni, K. A. and Davis, W. D., "The Use of Computer Models to Predict Temperature and Smoke Movement in High Bay Spaces", National Institute of Standards and Technology, NISTIR 5304, 1993.

[5] Heskestad, G., "Engineering Relations for fire Plumes", *Fire Safety Journal*, 7, pp 25-32, 1984.

[6] McCaffrey, B. J. "Purely Buoyant Diffusion Flames: Some Experimental Results." National Institute of Standards and Technology, NBSIR 79-1910, 1979.

[7] Alpert, R. L. , "Calculation of Response Time of Ceiling-Mounted Fire Detectors", *Fire Tech.*, 8,181 (1972).

[8] Peacock, R. D., Forney, G. P., Reneke, P., Portier, R., and Jones, W. W., "CFAST, The Consolidated Model of Fire Growth and Smoke Transport", National Institute of Standards and Technology, NIST Technical Note 1299, 1993.

[9] Deal, Scot, "Technical Reference Guide for FPEtool, Version 3.2", National Institute of Standards and Technology, NISTIR 5486-1, 1995

[10] Davis, W. D., and Cooper, L. Y., "Estimating the Environment and the Response of Sprinkler Links in Compartment Fires with Draft Curtains and Fusible Link-Actuated Ceiling Vents - Part II: User Guide for the Computer Code LAVENT", National Institute of Standards and Technology, NISTIR 89-4122, 1989.

[11] HARWELL FLOW3D, Release 3.2: User Manual, CFD Department, AEA Industrial Technology, Harwell Laboratory, Oxfordshire, United Kingdom. October, 1992.

[12] McGrattan, K.B.,Rehm, R. G. and Baum, H.R., "Fire Driven flows in Enclosures", *Journal of Computational Physics*, 110, 285 1994.

[13] Forney, G. P., and Moss, W. F., "Analyzing and Exploiting Numerical Characteristics of Zone Fire Models", *Fire Science & Technology* Vol. 14 No. 1 & No. 2 (49-60)1994

[14] Launder, B., E. and Spalding, D.,B., "The Numerical Computation of Turbulent Flows", *Computer Methods in Applied Mechanics and Engineering* 3 (1974) 269-289 North-Holland Publishing Company.

[15] Evans, D. D. and Stroup, D. W., "Methods to Calculate the Response Time of Heat and Smoke Detectors Installed Below Large Unobstructed Ceilings", *Fire Tech.*, 22, 54 (1986).

[16] McCaffrey, B. J., "Momentum Implications for Buoyant Diffusion Flames", *Combustion and Flame* 52,149(1983).

[17] Cooper, L. Y., "Fire-Plume-Generated Ceiling Jet Characteristics and Convective Heat Transfer to Ceiling and Wall Surfaces in a Two-Layer Zone-Type Fire Environment", National Institute of Standards and Technology, NISTIR 4705, 1991.

[18] Portier, Rebecca W., Peacock, Richard D., and Reneke, Paul A., "FASTLite: Engineering Tools for Estimating Fire Growth and Smoke Transport", National Institute of Standards and Technology, NIST Special Publication 899, Gaithersburg, MD,(1996)

[19] Forney, Glenn, P. Private Communication

[20] Alpert, R.L., and Ward, E.J., "Evaluating Unsprinklered Fire Hazards", *SFPE Technology* Report 83-2, Society of Fire Protection Engineers, Boston, MA, 1983.

[21] Walton, W. D., "ASET-B, A Room Fire Program for Personal Computers", National Institute of Standards and Technology, NBSIR 85-3144, Gaithersburg, MD, 1985.

[22] Cooper, L. Y., "Estimating the Environment and the Response of Sprinkler Links in Compartment Fires with Draft Curtains and Fusible Link-Actuated Ceiling Vents - Part 1: Theory", National Institute of Standards and Technology, NBSIR 88-3734, Gaithersburg, MD, 1988.

[23] Rehm, R.G. and Baum, H.R., "The Equations of Motion for Thermally Driven, Buoyant Flows". *Journal of Research of the NBS*, 83, 297 1978.

[24] Heskestad, G., Delicatsios, M.A., "Environments of Fire Detectors--Phase I. Effect of Fire Size, Ceiling Height and Material", National Institute of Standards and Technology, NBS-GCR-77-86, Gaithersburg, MD 20899, 1977

[25] Baum, H. R., Ezekoye, O. A., McGrattan, K. B. and Rehm, R. G., "Mathematical Modeling and Computer Simulation of Fire Phenomena". *Theoretical and Computational Fluid Dynamics*, 6,(1994) 125-139.

Nomenclature

c_p	specific heat at constant pressure(J/mole K)
D	fire diameter(m)
g	acceleration of gravity(m/s^2)
H	ceiling height(m)
k	turbulent kinetic energy(J)
$\dot{m}_e$	entrained mass (kg/s)
P_o	average pressure (Pa)
$\dot{Q}$	total heat release rate (kW)
$\dot{Q}_c$	convective heat release rate (kW)
r	radial distance from fire center (m)
R	ideal gas constant (J/mole K)
T	temperature (K)
T_u	upper layer temperature (K)
T_l	lower layer temperature (K)
T_∞	ambient temperature (K)
u	gas velocity (m/s)
V	volume (m^3)
z	height above fire source (m)
z_o	virtual origin above fire source (m)
ϵ	turbulence dissipation rate (J/s)
μ	laminar viscosity (kg/m s)
μ_T	turbulent viscosity (kg/m s)
ρ_∞	ambient gas density (kg/m^3)

Appendix A

k-ε Model used in the CFD model CFX

The k-ε model uses an eddy-viscosity hypothesis for the turbulence in which the effective viscosity is the sum of the molecular laminar viscosity and the turbulent viscosity. The turbulent viscosity is calculated using

$$\mu_T = C_\mu \rho k^2/\epsilon \tag{14}$$

where μ_T is the turbulent viscosity, ρ is the gas density, k is the turbulence kinetic energy, and ϵ is the turbulence dissipation rate. Following the notation in the HARWELL FLOW3D USERS GUIDE [11], the transport equations for the turbulence kinetic energy and turbulence dissipation rate are:

$$\frac{\partial(\rho k)}{\partial t} + \nabla \cdot ((\mu + \frac{U_T}{\sigma_k})\nabla k) = P + G - \rho\epsilon \tag{15}$$

and

$$\frac{\partial \rho\epsilon}{\partial t} + \nabla \cdot (\rho U\epsilon) - \nabla\cdot((\mu + \frac{\mu_T}{\sigma_\epsilon})\nabla\epsilon) = C_1\frac{\epsilon}{k}(P + C_3 G) - C_2\rho\frac{\epsilon^2}{k} \tag{16}$$

where P is the shear production and G is the buoyancy production. The constants C_1, C_2, C_3, and C_μ as well as the turbulent Prandtl number σ_ϵ are set by the user. For the present calculations, the values used for C_1, C_2, C_3, C_μ and σ_ϵ are 1.44, 1.92, 1.0, 0.18, and 0.85 respectively.

Near boundaries or solids, wall functions are used to model the behavior of the flow in order to avoid using large numbers of control volumes. Details of these equations may be found in the users manual and a discussion of wall functions is available in reference [14]

Appendix B

Tables 1 - 6 provide the experimental measurements and model predictions for the radial temperature 0.31 m beneath the ceiling at the designated radial distances from the plume center. Tables 7 and 8 give the ceiling jet temperature measurements as a function of depth beneath the ceiling at 6.1 m and 9.1 m from the plume center. The model predictions to compare with these measurements are given in tables 9 - 12. Tables 13 and 14 provide the smoke detector activation times and activation temperatures.

Table 1: Radial temperatures for the 500 kW fire at 75 s

Radius	1.5 m	3.0 m	6.1 m	8.5 m	9.1 m	11.6 m
Exp. °C N - S	38 ± 2	37 ± 2	36 ± 2	33 ± 2	n.a.	n.a.
Exp. °C E - W	37 ± 2	35 ± 2	32 ± 2	31 ± 2	31 ± 2	30 ± 2
DETACT °C	37	35	32	31	31	31
CFAST °C	n.a.	39	39	38	38	37
FPEtool °C	n.a.	39	35	33	33	32
FPEtool Fir. S. °C	n.a.	39	38	37	37	37
LAVENT °C	37	37	37	36	36	35
CFX °C N	38	36	34	33	33	29
CFX °C E-W	38	37	35	34	32	28
NIST-LES °C	40	38	37	36	36	32

n. a. means not applicable.

Table 2: Radial temperatures for the 500 kW fire at 150 s

Radius	1.5 m	3.0 m	6.1 m	8.5 m	9.1 m	11.6 m
Exp. °C N - S	38 ± 2	38 ± 2	36 ± 2	36 ± 2	n.a.	n.a.
Exp. °C E - W	39 ± 2	37 ± 2	34 ± 2	34 ± 2	33 ± 2	30 ± 2
DETACT °C	39	38	34	33	33	32
CFAST °C	n.a.	41	42	41	41	41
FPEtool °C	n.a.	41	36	34	34	33
FPEtool Fir. S. °C	n.a.	41	39	38	38	37
LAVENT °C	41	41	40	39	39	38
CFX °C N	42	39	37	37	37	30
CFX °C E - W	42	40	38	38	37	30
NIST-LES °C	43	40	39	39	39	33

n .a. means not applicable.

Table 3: Radial temperatures for the 500 kW fire at 225 s

Radius	1.5 m	3.0 m	6.1 m	8.5 m	9.1 m	11.6 m
Exp °C N - S	40 ± 2	40 ± 2	37 ± 2	36 ± 2	n.a.	n.a.
Exp °C E - W	41 ± 2	39 ± 2	36 ± 2	35 ± 2	35 ± 2	32 ± 2
DETACT °C	40	39	35	33	33	32
CFAST °C	n.a.	41	41	41	41	41
FPEtool °C	n.a.	42	36	35	34	34
FPEtool Fir. S. °C	n.a.	42	39	39	39	38
LAVENT °C	42	42	42	41	41	40
CFX °C N	42	40	39	38	38	31
CFX °C E-W	42	41	40	39	38	30
NIST-LES °C	45	41	42	41	41	35

n. a. means not applicable.

Table 4: Radial temperatures for the 2.7 MW fire at 75 s

Radius	1.5 m	3.0 m	6.1 m	8.5 m	9.1 m	11.6 m
Exp °C N - S	62 ± 2	56 ± 2	44 ± 2	44 ± 2	n.a.	n.a.
Exp °C E - W	64 ± 2	56 ± 3	44 ± 4	40 ± 2	38 ± 2	30 ± 2
DETACT °C	55	53	43	40	39	38
CFAST °C	n.a.	63	64	62	62	61
FPEtool °C	n.a.	61	48	44	43	41
FPEtool Fir. S. °C	n.a.	60	55	53	52	51
LAVENT °C	58	58	57	55	55	53
CFX °C N	54	49	45	44	44	33
CFX °C E-W	54	51	48	46	45	28
NIST-LES °C	69	61	59	56	56	45

n. a. means not applicable.

Table 5: Radial temperatures for the 2.7 MW fire at 150 s

Radius	1.5 m	3.0 m	6.1 m	8.5 m	9.1 m	11.6 m
Exp °C N - S	68 ± 3	64 ± 2	55 ± 2	52 ± 2		
Exp °C E - W	67 ± 4	63 ± 4	54 ± 5	50 ± 2	49 ± 2	40 ± 2
DETACT °C	61	58	46	43	42	40
CFAST °C	n.a.	74	77	75	75	74
FPEtool °C	n.a.	67	52	47	46	43
FPEtool Fi. S. °C	n.a.	66	60	58	57	56
LAVENT °C	69	69	67	65	64	63
CFX °C N	63	58	53	52	52	40
CFX °C E-W	63	59	55	54	53	34
NIST-LES °C	81	74	70	68	68	54

n. a. means not applicable.

Table 6: Radial temperatures for the 2.7 MW fire at 225 s

Radius	1.5 m	3.0 m	6.1 m	8.5 m	9.1 m	11.6 m
Exp °C N - S	67 ± 4	64 ± 2	56 ± 2	54 ± 2	n.a.	n.a.
Exp °C E - W	66 ± 2	62 ± 2	58 ± 2	54 ± 2	52 ± 2	41 ± 3
DETACT °C	63	61	48	44	43	41
CFAST °C	n.a.	80	83	82	82	81
FPEtool °C	n.a.	70	54	49	48	44
FPEtool Fir. S. °C	n.a.	70	63	60	60	58
LAVENT °C	74	74	73	70	69	68
CFX °C N	66	60	56	55	55	41
CFX °C E-W	65	62	58	57	56	36
NIST-LES °C	83	76	73	74	74	55

n. a. means not applicable.

Table 7: Ceiling Jet temperature as a function of distance beneath the ceiling for the 500 kW fire

Time s	Depth m	North 6.1 m	South 6.1 m	West 6.1 m	East 6.1 m	East 9.1 m
75	0.15	36 ± 1	35 ± 1	31 ± 1	34 ± 1	31 ± 1
	0.3	36 ± 1	34 ± 1	33 ± 1	34 ± 1	32 ± 1
	0.46	33 ± 1	34 ± 1	33 ± 1	34 ± 1	32 ± 1
	0.61	34 ± 1	34 ± 1	33 ± 1	34 ± 1	32 ± 1
	0.76	33 ± 1	34 ± 1	33 ± 1	34 ± 1	32 ± 1
	Depth m					
150	0.15	37 ± 1	35 ± 1	31 ± 1	35 ± 1	31 ± 1
	0.3	37 ± 1	34 ± 1	33 ± 1	36 ± 1	32 ± 1
	0.46	35 ± 1	34 ± 1	33 ± 1	36 ± 1	32 ± 1
	0.61	36 ± 1	34 ± 1	33 ± 1	36 ± 1	32 ± 1
	0.76	37 ± 1	34 ± 1	33 ± 1	36 ± 1	32 ± 1
	Depth m					
225	0.15	37 ± 1	37 ± 1	35 ± 1	36 ± 1	35 ± 1
	0.3	37 ± 1	37 ± 1	37 ± 1	37 ± 1	34 ± 1
	0.46	35 ± 1	37 ± 1	38 ± 1	37 ± 1	35 ± 1
	0.61	37 ± 1	37 ± 1	37 ± 1	37 ± 1	36 ± 1
	0.76	36 ± 1	37 ± 1	37 ± 1	37 ± 1	36 ± 1

Table 8: Ceiling Jet temperature as a function of distance beneath the ceiling for the 2.7 MW fire

Time s	Depth m	North 6.1 m	South 6.1 m	West 6.1 m	East 6.1 m	East 9.1 m
75	0.15	43 ± 1	46 ± 1	39 ± 1	52 ± 1	41 ± 1
	0.3	44 ± 1	49 ± 1	45 ± 1	51 ± 1	42 ± 1
	0.46	44 ± 1	49 ± 1	46 ± 1	52 ± 1	43 ± 1
	0.61	46 ± 1	49 ± 1	45 ± 1	54 ± 1	43 ± 1
	0.76	47 ± 1	47 ± 1	46 ± 1	54 ± 1	42 ± 1
	Depth m					
150	0.15	51 ± 1	51 ± 1	47 ± 1	61 ± 1	52 ± 1
	0.3	50 ± 1	57 ± 1	53 ± 1	61 ± 1	51 ± 1
	0.46	50 ± 1	58 ± 1	54 ± 1	60 ± 1	52 ± 1
	0.61	52 ± 1	57 ± 1	55 ± 1	59 ± 1	54 ± 1
	0.76	56 ± 1	57 ± 1	54 ± 1	57 ± 1	54 ± 1
	Depth m					
225	0.15	52 ± 1	56 ± 1	50 ± 1	63 ± 1	55 ± 1
	0.3	52 ± 1	62 ± 1	57 ± 1	63 ± 1	55 ± 1
	0.46	52 ± 1	63 ± 1	58 ± 1	61 ± 1	57 ± 1
	0.61	55 ± 1	63 ± 1	58 ± 1	60 ± 1	57 ± 1
	0.76	58 ± 1	62 ± 1	59 ± 1	58 ± 1	55 ± 1

Table 9: Ceiling jet zone model predictions for the 500 kW fire

Time s	Model	CFAST 6.1 m	LAVENT 6.1 m	CFAST 9.1 m	LAVENT 9.1 m
75	Depth m				
	0.15	36 °C	37 °C	35 °C	35 °C
	0.30	36 °C	37 °C	35 °C	36 °C
	0.46	35 °C	36 °C	35 °C	36 °C
	0.61	34 °C	35 °C	35 °C	35 °C
	0.76	33 °C	35 °C	34 °C	35 °C
150	Depth m				
	0.15	41 °C	40 °C	38 °C	38 °C
	0.30	40 °C	41 °C	39 °C	39 °C
	0.46	39 °C	41 °C	39 °C	39 °C
	0.61	37 °C	40 °C	38 °C	38 °C
	0.76	36 °C	40 °C	37 °C	38 °C
225	Depth m				
	0.15	43 °C	42 °C	40 °C	39 °C
	0.30	42 °C	42 °C	41 °C	41 °C
	0.46	41 °C	41 °C	41 °C	40 °C
	0.61	39 °C	40 °C	40 °C	40 °C
	0.76	37 °C	39 °C	39 °C	40 °C

Table 10: Ceiling jet field model predictions for the 500 kW fire

Time s	Model	CFX 6.1 m N	CFX 6.1 m E	CFX 9.1 m E	NIST-LES 6.1 m	NIST-LES 9.1 m
75	Depth m					
	0.15	34 °C	35 °C	33 °C	37 °C	36 °C
	0.30	34 °C	35 °C	34 °C	37 °C	36 °C
	0.46	33 °C	35 °C	34 °C	36 °C	35 °C
	0.61	33 °C	35 °C	34 °C	35 °C	34 °C
	0.76	33 °C	34 °C	34 °C	34 °C	33 °C
150	Depth m					
	0.15	38 °C	39 °C	38 °C	39 °C	39 °C
	0.30	37 °C	39 °C	38 °C	39 °C	39 °C
	0.46	37 °C	39 °C	38 °C	38 °C	38 °C
	0.61	37 °C	39 °C	38 °C	37 °C	37 °C
	0.76	37 °C	38 °C	38 °C	36 °C	36 °C
225	Depth m					
	0.15	39 °C	40 °C	39 °C	42 °C	41 °C
	0.30	39 °C	40 °C	39 °C	42 °C	41 °C
	0.46	39 °C	40 °C	39 °C	41 °C	40 °C
	0.61	39 °C	40 °C	39 °C	40 °C	39 °C
	0.76	39 °C	40 °C	39 °C	39 °C	38 °C

Table 11: Ceiling jet zone model predictions for the 2.7 MW fire

Time s	Model	CFAST 6.1 m	LAVENT 6.1 m	CFAST 9.1 m	LAVENT 9.1 m
75	Depth m				
	0.15	65 °C	58 °C	58 °C	52 °C
	0.3	64 °C	57 °C	62 °C	54 °C
	0.46	60 °C	55 °C	61 °C	54 °C
	0.61	55 °C	53 °C	58 °C	53 °C
	0.76	51 °C	50 °C	56 °C	51 °C
150	Depth m				
	0.15	78 °C	68 °C	70 °C	61 °C
	0.30	76 °C	67 °C	75 °C	64 °C
	0.46	72 °C	65 °C	73 °C	63 °C
	0.61	66 °C	62 °C	70 °C	62 °C
	0.76	61 °C	60 °C	67 °C	61 °C
225	Depth m				
	0.15	84 °C	71 °C	75 °C	65 °C
	0.30	82 °C	71 °C	81 °C	69 °C
	0.46	77 °C	68 °C	79 °C	69 °C
	0.61	71 °C	65 °C	74 °C	68 °C
	0.76	66 °C	63 °C	72 °C	66 °C

Table 12: Ceiling jet field model predictions for the 2.7 MW fire

Time s	Model	CFX 6.1 m N	CFX 6.1 m E	CFX 9.1 m E	NIST-LES 6.1 m	NIST-LES 9.1 m
75	Depth m					
	0.15	45 °C	48 °C	45 °C	59 °C	56 °C
	0.30	45 °C	48 °C	45 °C	58 °C	56 °C
	0.46	45 °C	48 °C	45 °C	56 °C	54 °C
	0.61	44 °C	47 °C	45 °C	55 °C	52 °C
	0.76	44 °C	47 °C	45 °C	54 °C	50 °C
150	Depth m					
	0.15	53 °C	55 °C	53 °C	70 °C	68 °C
	0.30	53 °C	55 °C	53 °C	70 °C	68 °C
	0.46	53 °C	55 °C	53 °C	68 °C	67 °C
	0.61	53 °C	55 °C	53 °C	67 °C	66 °C
	0.76	52 °C	55 °C	53 °C	66 °C	64 °C
225	Depth m					
	0.15	56 °C	58 °C	56 °C	73 °C	74 °C
	0.30	56 °C	58 °C	56 °C	73 °C	74 °C
	0.46	56 °C	58 °C	56 °C	72 °C	73 °C
	0.61	56 °C	58 °C	56 °C	71 °C	72 °C
	0.76	56 °C	58 °C	56 °C	69 °C	69 °C

Table 13: Smoke detector activation
for the 500 kW fire

Radius	3.0 m	6.1 m	8.5 m	9.1 m	11.6 m	13.7 m
Time N	27 s	44 s	40 s			
Temp. N	6 °C	5 °C	3 °C			
Time E	23 s	35 s		73 s	90 s	181 s
Temp. E	5 °C	1 °C		3 °C	3 °C	
Time S	32 s	53 s	48 s			
Temp. S	6 °C	5 °C	3 °C			
Time W	31 s	60 s		81 s	90 s	173 s
Temp. W	5 °C	4 °C		4 °C	4 °C	2 °C

Table 14: Smoke detector activation
for the 2.7 MW fire

Radius	3.0 m	6.1 m	8.5 m	9.1 m	11.6 m	13.7 m
Time N	25 s	30 s	38 s			
Temp. N	4 °C	7 °C	3 °C			
Time E	17 s	22 s		29 s	38 s	67 s
Temp. E	1 °C	1 °C		1 °C	1 °C	2 °C
Time S	26 s	26 s	30 s			
Temp. S	7 °C	1 °C	2 °C			
Time W	21 s	29 s		38 s	46 s	58 s
Temp. W	1 °C	1 °C		1 °C	1 °C	1 °C

NIST-114
(REV. 6-93)
ADMAN 4.09

U.S. DEPARTMENT OF COMMERCE
NATIONAL INSTITUTE OF STANDARDS AND TECHNOLOGY

MANUSCRIPT REVIEW AND APPROVAL

ERB CONTROL NUMBER	DIVISION
	865
PUBLICATION REPORT NUMBER	CATEGORY CODE
NISTIR 5927	
PUBLICATION DATE	NUMBER PRINTED PAGES
December 1996	

INSTRUCTIONS: ATTACH ORIGINAL OF THIS FORM TO ONE (1) COPY OF MANUSCRIPT AND SEND TO THE SECRETARY, APPROPRIATE EDITORIAL REVIEW BOARD

TITLE AND SUBTITLE (CITE IN FULL)

Comparison of Fire Model Predictions with Experiments Conducted in a Hangar with a 15 meter Ceiling

CONTRACT OR GRANT NUMBER	TYPE OF REPORT AND/OR PERIOD COVERED

AUTHOR(S) (LAST NAME, FIRST INITIAL, SECOND INITIAL)

Davis, W. D., Notarianni, K. A., and McGrattan, K. B.

PERFORMING ORGANIZATION (CHECK (X) ONE BOX)

- [x] NIST/GAITHERSBURG
- [ ] NIST/BOULDER
- [ ] JILA/BOULDER

LABORATORY AND DIVISION NAMES (FIRST NIST AUTHOR ONLY)

Building and Fire Research Laboratory, Fire Safety Engineering Division

SPONSORING ORGANIZATION NAME AND COMPLETE ADDRESS (STREET, CITY, STATE, ZIP)

National Aeronautics and Space Administration
NASA Headquarters

NIST Category No.
NIST- 240

PROPOSED FOR NIST PUBLICATION

- [ ] JOURNAL OF RESEARCH (NIST JRES)
- [ ] J. PHYS. & CHEM. REF. DATA (JPCRD)
- [ ] HANDBOOK (NIST HB)
- [ ] SPECIAL PUBLICATION (NIST SP)
- [ ] TECHNICAL NOTE (NIST TN)
- [ ] MONOGRAPH (NIST MN)
- [ ] NATL. STD. REF. DATA SERIES (NIST NSRDS)
- [ ] FEDERAL INF. PROCESS. STDS. (NIST FIPS)
- [ ] LIST OF PUBLICATIONS (NIST LP)
- [x] NIST INTERAGENCY/INTERNAL REPORT (NISTIR)
- [ ] LETTER CIRCULAR
- [ ] BUILDING SCIENCE SERIES
- [ ] PRODUCT STANDARDS
- [ ] OTHER

PROPOSED FOR NON-NIST PUBLICATION (CITE FULLY) [x] U.S. [ ] FOREIGN

PUBLISHING MEDIUM

- [x] PAPER
- [ ] CD-ROM
- [ ] DISKETTE (SPECIFY)
- [ ] OTHER (SPECIFY)

SUPPLEMENTARY NOTES

ABSTRACT (A 2000-CHARACTER OR LESS FACTUAL SUMMARY OF MOST SIGNIFICANT INFORMATION. IF DOCUMENT INCLUDES A SIGNIFICANT BIBLIOGRAPHY OR LITERATURE SURVEY, CITE IT HERE. SPELL OUT ACRONYMS ON FIRST REFERENCE.) (CONTINUE ON SEPARATE PAGE, IF NECESSARY.)

The National Aeronautics and Space Administration, together with the National Institute of Standards and Technology are in the fourth year of a five year project designed to help NASA set guidelines for fire protection in high bay facilities. A high bay facility is defined in this study as any space with a ceiling height in excess of 9 m. NASA has numerous high bay spaces that are used to perform a variety of functions. The work this year made use of a set of fire experiments conducted in a 15 m high hangar by NIST and the US Navy to study the predictive capabilities of zone fire models and computational fluid dynamics models (CFD). The models studied included the zone models CFAST, DETACT-QS, FPETool, and LAVENT and the CFD models CFX and NIST-LES. The study compares the model predictions with measured temperature profiles in the ceiling jet and the plume. Velocity measurements, smoke detector activation and the impact of draft curtains on smoke flow are also analyzed. The fires sizes studied in the experiment are 500 kW and 2.7 MW JP-5 pan fires.

KEY WORDS (MAXIMUM OF 9; 28 CHARACTERS AND SPACES EACH; SEPARATE WITH SEMICOLONS; ALPHABETIC ORDER; CAPITALIZE ONLY PROPER NAMES)

CFD models; experiments; fire models; fire simulation; fire tests; heat detection; high bays; smoke detection; zone models

AVAILABILITY

- [x] UNLIMITED
- [ ] FOR OFFICIAL DISTRIBUTION - DO NOT RELEASE TO NTIS
- [ ] ORDER FROM SUPERINTENDENT OF DOCUMENTS, U.S. GPO, WASHINGTON, DC 20402
- [x] ORDER FROM NTIS, SPRINGFIELD, VA 22161

NOTE TO AUTHOR(S): IF YOU DO NOT WISH THIS MANUSCRIPT ANNOUNCED BEFORE PUBLICATION, PLEASE CHECK HERE. [ ]

WORDPERFECT